A SEASONAL THREE-DIMENSIONAL ECOSYSTEM MODEL OF NITROGEN CYCLING IN THE NORTH ATLANTIC EUPHOTIC ZONE

J. L. Sarmiento,[1] R. D. Slater,[1] M. J. R. Fasham,[2] H. W. Ducklow,[3] J. R. Toggweiler,[4] and G. T. Evans [5]

Abstract. A seven-component upper ocean ecosystem model of nitrogen cycling calibrated with observations at Bermuda Station "S" has been coupled to a three-dimensional seasonal general circulation model (GCM) of the North Atlantic ocean. The aim of this project is to improve our understanding of the role of upper ocean biological processes in controlling surface chemical distributions, and to develop approaches for assimilating large data sets relevant to this problem. A comparison of model predicted chlorophyll with satellite coastal zone color scanner observations shows that the ecosystem model is capable of responding realistically to a variety of physical forcing environments. Most of the discrepancies identified are due to problems with the GCM model. The new production predicted by the model is equivalent to 2 to 2.8 mol m^{-2} yr^{-1} of carbon uptake, or 8 to

[1]Program in Atmospheric and Oceanic Sciences, Princeton University, Princeton, New Jersey.

[2]Institute of Oceanographic Sciences Deacon Laboratory, Natural Environmental Research Council, Southampton SO1 7NS, United Kingdom.

[3]Horn Point Environmental Laboratories, University of Maryland Center for Environmental and Estuarine Sciences Cambridge, Maryland.

[4]Geophysical Fluid Dynamics Laboratory, NOAA, Princeton University, Princeton, New Jersey.

[5]Department of Fisheries and Oceans, Science Branch St. John's, Newfoundland, Canada.

12 GtC/yr on a global scale. The southern half of the subtropical gyre is the only major region of the model with almost complete surface nitrate removal (nitrate<0.1 mmol m^{-3}). Despite this, almost the entire model is nitrate limited in the sense that any addition of nitrate supply would go predominantly into photosynthesis. The only exceptions are some coastal upwelling regions and the high latitudes during winter, where nitrate goes as high as ~10 mmol m^{-3}.

1. INTRODUCTION

A daunting prospect faces anyone attempting to understand the cycling of chemicals in the ocean. Circulation thwarts attempts to carry out controlled measurements in manageable portions of the ocean, and we understand only poorly the myriad effects of biology. A brief catalog of major issues relating to just one aspect of the biological pump, namely the formation of organic matter at the surface and its export to depth, serves to illustrate the problem:

What controls the production of organic matter in the surface ocean and the effect of this on surface properties? In most regions of the ocean, nitrate supply is thought to limit the production of organic matter, but in vast areas the concentration of nitrate is well in excess of that required to sustain growth [e.g., Chisholm and Morel, 1991]. It has been suggested that the fluctuations in surface carbon content that would result from postulated variations in nutrient content in one of these areas, the southern ocean, may have caused the large changes in atmospheric carbon dioxide that occurred during the last ice age [e.g., Knox and McElroy, 1984; Sarmiento and Toggweiler, 1984; Siegenthaler and Wenk, 1984]. Recent observations suggesting that iron limits growth [Martin and Fitzwater, 1988; Martin et al., 1990] remain controversial [e.g., Banse, 1990; Chisholm and Morel, 1991].

What is the export of organic carbon from the surface? Estimates range from as low as 3.4 to 7.4 GtC/a (1 Gt = 10^{12} kg [Eppley, 1989] to as high as 20 GtC/a [Packard et al., 1988]. One could obtain a measure of the organic carbon export from estimates of the net transport of inorganic carbon into the surface ocean from below, but this quantity is poorly known as well. Information on spatial and temporal variability is scanty.

How does organic matter leave the surface? It had been thought that it left primarily as sinking particles [e.g., Eppley and Peterson, 1979], but recent measurements of dissolved organic matter [Suzuki et al., 1985; Sugimura and Suzuki, 1988; Toggweiler, 1989] led to suggestions that particles might account for less than half the total. Subsequent work has failed to confirm these high dissolved organic matter concentrations [e.g., Benner et al., 1992; Ogawa and Ogura, 1992]. However, model studies appear to require that a substantial fraction of the organic matter be exported in the dissolved form so as to avoid trapping of nutrients under regions of high productivity [Bacastow and Maier-Reimer, 1991; Najjar et al., 1992].

How is the export of organic matter from the surface (export production, which is equal to the new production in steady state) related to the total rate at which photosynthesis occurs (primary production)? The export of organic matter is the process of most importance in understanding the impact of biology on the distribution of chemicals in the ocean. However, primary production is the process we understand the best, and the one quantity there is some promise of being able to estimate on a global scale from satellite color observations [e.g., Platt et al., 1992]. The ratio of the new production to the primary production, often referred to as the "f ratio" is as yet poorly sampled.

We discuss here an attempt to address these and related important issues through the development of a coupled model of ocean circulation, biology, and chemistry based on primitive equation ocean general circulation models (GCMs) of the type first developed by Bryan [1969]. Despite their well-known difficulties, GCMs provide a powerful tool for improving our insight into how the oceans function. GCMs have been used before to study the cycling of nutrients in the open ocean [e.g., Maier-Reimer and Hasselman, 1987; Bacastow and Maier-Reimer, 1990, 1991; Najjar et al., 1992], but in all these cases the role of biology was parameterized in a simple way that ignored the complexity of the processes occurring. Ecosystem models trace the cycling of chemicals from their uptake in the inorganic form, through their incorporation by organisms into organic matter, then back to the inorganic form [Riley, 1947; Steele, 1958; Wroblewski, 1977; Toggweiler et al., 1987]. We employ a recently developed version of these models [Fasham et al., 1990], (here-in-after referred to as FDM, 1990) to attempt for the first time to incorporate realistic biology directly into open ocean GCM models of nutrient cycling. Similar regional models include studies by Wroblewski [1977], Walsh and McRoy [1986], Hofmann [1988], and Walsh et al. [1988].

The approach we followed was to develop a simple, easily modified nitrogen-based model of ecosystem dynamics for the oceanic mixed layer (FDM, 1990), then incorporate this biogeochemical submodel into a basin-scale seasonal Atlantic Ocean GCM developed earlier at Princeton [Sarmiento, 1986].

Our long term goal is to develop a single generic ecosystem model that can be applied throughout the entire model domain, the local manifestations of which would thus be determined by differences in the physical forcing. The ecosystem model we used was calibrated with observations at Bermuda Station "S" (FDM, 1990), but has been been shown to work reasonably well at a variety of other locations as well. The FDM(1990) ecosystem model, which is aimed primarily at addressing the production of organic matter in the surface ocean and its export to depth, is solved in the upper 123 m of the water column. It achieves repeating annual cycles superimposed on a slow long term drift within less than two years. Our analysis of the simulations is carried out using results from the third year. The effect of regeneration of organic matter on the concentration of nitrate below 123 m takes decades to centuries to adjust and is reflected at the surface by a slow long-term drift which would be expected to be relatively insensitive to the details of the regeneration parameterization on a time scale of a few years. We thus use a simple parameterization for regeneration, based in part on empirical observations of the decrease in particle flux with depth. The problem of developing realistic simulations of the regeneration processes is being addressed in separate model studies involving simulations of more than 1000 years [e.g., Najjar et al., 1992].

Although this first model is focussed on nitrogen, our long-term goals are centered primarily on understanding the cycling of carbon dioxide, nitrous oxide, and dimethyl sulphide (DMS), because of the major role they play in controlling climate; and on developing a model for assimilation of satellite color observations as a technique for long-term monitoring of biological productivity and fluxes. We use nitrogen for our initial work because this allows us to separate nitrate-based new production from ammonium-based regenerated production in our model [Dugdale and Goering, 1967]. Furthermore, in any successful model of biology the processes limiting growth must be included explicitly. Nitrogen supply is thought to be the major limit to biological production over much of the ocean [Carpenter and Capone, 1983]. One of the most important things we look for in our model is evidence supporting this view, as well as evidence that processes other than nitrogen supply (e.g., irradiance, grazing) are limiting biological production.

2. MODEL DESCRIPTION

We provide only a brief discussion of the GCM and ecosystem models used in this simulation, referring the reader to Sarmiento [1986] for a more detailed discussion of the GCM, and to FDM(1990) and Fasham [1993] for a discussion of the upper ocean ecosystem model, including a justification for the form of the ecosystem chosen and the values of the parameters used. Fasham et al. (this issue) give an updated discussion of some aspects of the ecosystem model.

The ecosystem model consists of seven compartments describing phytoplankton, zooplankton, bacteria, nonliving particulate organic nitrogen (PON), and three forms of dissolved nitrogen: nitrate, ammonium, and organic (DON) (see Figure 1). FDM(1990) provide balance equations for each of these seven components, which consist primarily of terms describing their interactions. An additional term describes the
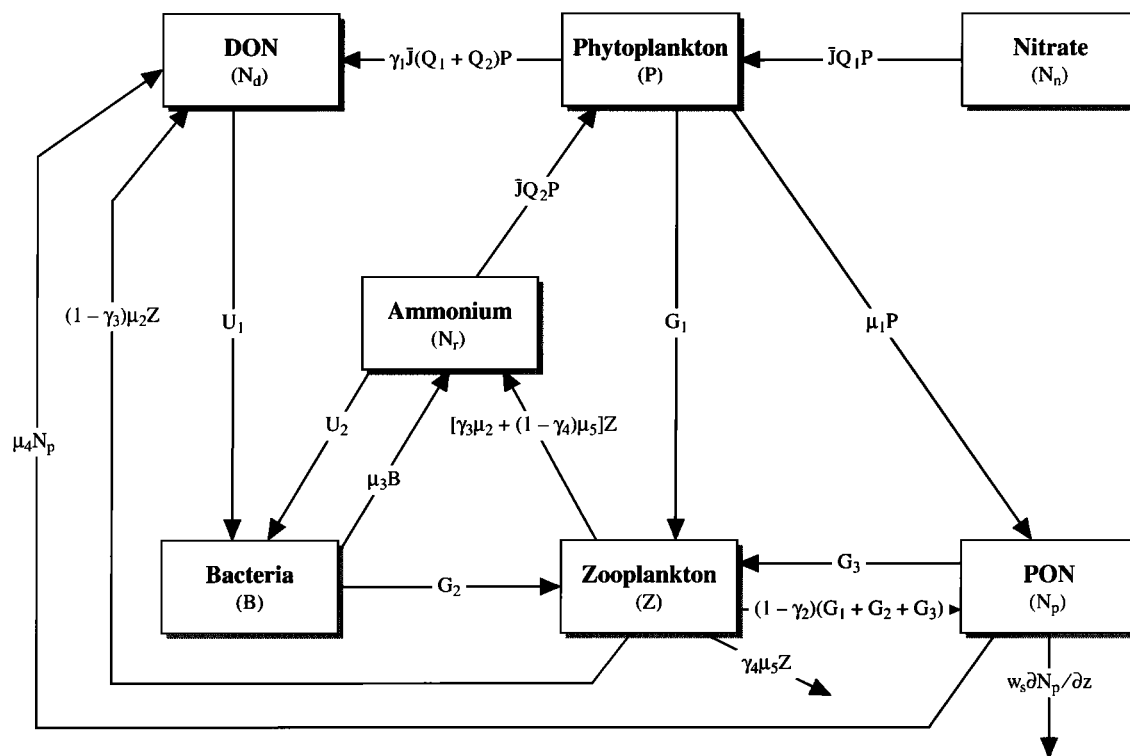
Fig. 1. The upper ocean ecosystem model. See text for a description of terms. PON is nonliving particulate organic nitrogen and DON is dissolved organic nitrogen.

role of vertical mixing. Incorporating these equations into our GCM entails using the same balance equation that predicts the effect of advection, diffusion, and convection on the distribution of heat and salt in the GCM, and adding to it the FDM(1990) biological terms that describe the interactions between the compartments. Initial and boundary conditions must be set, and we also must deal with regeneration of organic matter below 123 m. Details are given below.

2.1. GCM

We use a seasonal ocean general circulation model of the Atlantic from 30°S to 68°N with 2° horizontal resolution and 25 vertical levels (6 in the upper 123 m where the ecosystem equations are solved). Table 1 shows the bottom depths of the layers. The circulation is determined by solution of the equations of motion, state, and heat and salt balance as described by Sarmiento [1986]. Convective overturning is simulated by homogenizing adjacent layers when they are unstable with respect to each other. The model is forced at the surface with the monthly climatic average winds of Hellerman and Rosenstein [1983] and the monthly averaged temperatures and seasonally averaged salinities of Levitus [1982]. It is run for 500 years before being used for the ecosystem simulation. The ecosystem balance equations, given in the next section, are then solved simultaneously with the GCM equations.

The boundaries at 30°S and 68°N are closed walls, which the water is forced to flow along instead of through. We supress the distortions that this causes by adding a decay term

TABLE 1. Bottom Depths of Model Layers

Layer Number	Bottom Depth
1	10
2	23
3	40
4	61
5	88
6	123
7	166
8	220
9	287
10	369
11	468
12	588
13	732
14	903
15	1104
16	1339
17	1612
18	1926
19	2284
20	2690
21	3146
22	3654
23	4215
24	4831
25	5501

$\gamma(T^* - T)$ to the equation for temperature T (and a similar term for salinity), which restores it to the observed temperature field T^*. The value γ varies smoothly from 0.2 d^{-1} at the walls to zero 10 degrees away from them. This forcing enables conversion of surface waters to deep waters in the north and the reverse process in the south. The upwelling of deep waters across the high vertical density gradient in the south gives rise to high horizontal density gradients. These gradients and the flows they result in are suppressed with high lateral heat diffusivities and momentum viscosities, as explained by Sarmiento [1986].

2.2 . Ecosystem Model

Seven equations describe the flow of the components of the ecosystem depicted in Figure 1. They all take the form

$$0 = T(C_i) + SMS(C_i) \qquad i = 1...7 \qquad (1)$$

with

$$T(C_i) \equiv -\frac{\partial C_i}{\partial t} - \vec{V} \cdot \vec{\nabla} C_i + \vec{\nabla} \cdot \left(\frac{D}{\delta} \vec{\nabla} C_i \right)$$

C_i is the concentration in mmol m^{-3} of nitrogen of the ecosystem component in question. V is velocity and D is diffusion, both of which are provided by the GCM. The value $\delta = 1$ except when adjacent layers are unstable with respect to each other, in which case $\delta = 0$ (i.e., convection occurs). $SMS(C_i)$ are the biological interaction terms, with SMS symbolizing sources minus sinks.

In the upper 123 m where the ecosystem model is solved, the biological interaction terms are the following:

$$SMS(P) = (1 - \gamma_1)\bar{J}(z,t)[Q_1(N_n,N_r) + Q_2(N_r)]P - G_1 - \mu_1 P$$

$$SMS(Z) = \gamma_2(G_1 + G_2 + G_3) - (\mu_2 + \mu_5)Z$$

$$SMS(B) = U_1 + U_2 - G_2 - \mu_3 B$$

$$SMS(N_n) = -\bar{J}(z,t)Q_1(N_n,N_r)P \qquad (2)$$

$$SMS(N_r) = [\gamma_3\mu_2 + (1 - \gamma_4)\mu_5]Z + \mu_3 B$$
$$\qquad\qquad - \bar{J}(z,t)Q_2(N_r)P - U_2$$

$$SMS(N_d) = \gamma_1 \bar{J}(z,t)[Q_1(N_n,N_r) + Q_2(N_r)]P$$
$$\qquad\qquad + (1 + \gamma_3)\mu_2 Z + \mu_4 N_p - U_1$$

$$SMS(N_p) = \mu_1 P + (1 - \gamma_2)(G_1 + G_2 + G_3)$$
$$\qquad\qquad - G_3 - \mu_4 N_p - w_s \frac{\partial N_p}{\partial z}$$

P is phytoplankton, Z is zooplankton, B is bacteria, N_n is nitrogen in nitrate, N_r is nitrogen in ammonium, N_d is dissolved organic nitrogen, and N_p is nonliving particulate organic nitrogen. The subscripts n and r refer to the fact that nitrate nitrogen drives new production and ammonium nitrogen

drives regenerated production [Dugdale and Goering, 1967]. The coefficients γ, which are dimensionless, and μ, which have units of d^{-1}, are defined and values for them given in Table 2, along with values for all other parameters in the model. The value w_s is the sinking velocity of particulate organic nitrogen. Of the zooplankton loss term $\mu_5 Z$, a portion γ_4 represents rapidly sinking fecal material and corpses produced by higher order predators, and the remainder goes to ammonium. The $\gamma_4\mu_5 Z$, term is assumed to be instantly exported and is included directly in the regeneration equations below 123 m discussed below.

The remaining ecosystem interaction terms in (2) are given in the following equations. For phytoplankton uptake we have first the nondimensional nutrient limitation terms:

$$Q_1(N_n,N_r) = \frac{N_n}{K_1 + N_n} e^{-\psi N_r} \qquad (3)$$

$$Q_2(N_r) = \frac{N_r}{K_1 + N_r}$$

An exponential is included in the nitrate limitation term, Q_1, to account for ammonium inhibition. Next we have the light limited growth rate, J, with units of d^{-1}. Although it would be possible to do so, this version of our model does not resolve the day/night cycle. Instead we use the average of J, $\bar{J}$, over $\tau_0 =$ one day and model layer i:

$$\bar{J}(z,t) = \frac{1}{\tau_0} \int^{\tau_0} \frac{1}{\tilde{z}_i - \tilde{z}_{i+1}} \int_{\tilde{z}_{i+1}}^{\tilde{z}} J(z,t) dz\, dt \qquad (4)$$

where

$$J(z,t) = \frac{V_p \alpha I(z,t)}{[V_p^2 + (\alpha I(z,t))^2]^{1/2}}$$

$$I(z,t) = I(t)_{z=0} \exp\left(k_w \tilde{z} - \int_{\tilde{z}}^0 k_c P dz \right)$$

$$I(t)_{z=0} = PAR \cdot f_c(t) \cdot \tau(t) \cdot \tilde{I}_n(t)$$

$$V_p = ab^{cT}$$

$\tilde{z}$ is the effective vertical coordinate after allowing for a non-vertical noontime sun angle ($\tilde{z} = z/\sqrt{1 - (\cos\theta/1.33)^2}$ where θ is the angle of incidence and 1.33 is the index of refraction in water). V_p is the growth rate in d^{-1} as $I \to \infty$, and α is the initial slope of the photosynthesis versus irradiance (P-I) curve in d^{-1} (W m^{-2})$^{-1}$. The irradiance, $I(z,t)$, is given in units of W m^{-2} as a function of $I(t)_{z=0}$, the irradiance just below the surface of the ocean, and the light attenuation including the effect of self-shading by phytoplankton. k_w is the attenuation coefficient due to water, and k_c is the self shading parameter. $I(t)_{z=0}$ is a function of the clear sky irradiance at noon, $\tilde{I}_n(t)$, times the portion of the radiation that is photosynthetically active, PAR, a dimensionless correction term for the effect of cloud cover, $f_c(t)$, and a function defining the evolution of the day, $\tau(t)$.

TABLE 2. Model Parameters

Parameter	Symbol	Value	Units
Phytoplankton (P) Coefficients			
Exudation fraction	γ_1	0.05	
Specific mortality rate	μ_1	0.04	d^{-1}
Half-saturation constants for nutrient uptake	K_1, K_2	0.5	mmol m^{-3}
Ammonium inhibition parameter	ψ	1.5	(mmol m^{-3})$^{-1}$
Initial slope of P-I curve	α	0.025	d^{-1}/(W m^{-2})
Light attenuation due to water	k_w	0.04	m^{-1}
Light attenuation by phytoplankton	k_c	0.03	m^{-1} (mmol m^{-3})$^{-1}$
Photosynthetically active radiation	PAR	0.40	
Maximum growth rate parameters	a	0.6	d^{-1}
	b	1.066	
	c	1.0	(°C)$^{-1}$
Zooplankton (Z) Coefficients			
Assimilation efficiency	γ_2	0.75	
Ammonium fraction of Z excretion	γ_3	0.75	
Detrital fraction of Z mortality	γ_4	0.33	
Specific excretion rate	μ_2	0.1	d^{-1}
Specific mortality rate	μ_5	0.05	d^{-1}
Maximum growth rate	g	1.0	d^{-1}
Half-saturation for ingestion	K_3	1.0	mmol m^{-3}
Relative preference for phytoplankton	ρ_1	0.5	
Relative preference for bacteria	ρ_2	0.25	
Relative preference for particulate organic nitrogen	ρ_3	0.25	
Bacterial (B) Coefficients			
Specific excretion rate	μ_3	0.05	d^{-1}
Maximum growth rate	V_B	2.0	d^{-1}
Half-saturation rate for uptake	K_4	0.5	mmol m^{-3}
Ammonium/dissolved organic nitrogen uptake ratio	η	0.6	
Detrital (N_p) Coefficients			
Breakdown rate	μ_4	0.05	d^{-1}
Sinking velocity	w_s	-10.0	m d^{-1}
Coefficients for Regeneration Equations (Below 123 m)			
Decay rate	λ	0.1	d^{-1}
Detrital regeneration exponent	ν	0.858	

Cloud cover is taken from the atlas produced by Levitus (personal communication, 1988) with cloud transmittance treated as in the work by Smith and Dobson [1984]. $\tau(t)$. is given as a triangular function which increases linearly from 0 to 1 from daybreak to noon, then decreases linearly to 0 at nightfall. Evans and Parslow [1985] adopted this form so that they could obtain an analytical solution to the integral in (4). T is temperature in °C. Values of all the parameters and definitions and values of the parameters not discussed above, including the V_P parameters, a, b, and c [Eppley, 1972], are given in Table 2.

For zooplankton grazing we have

$$G_j = gZ \frac{p_j C_j}{K_3 + \sum_{k=1}^{k=3}(p_k C_k)} \qquad j = 1...3 \qquad (5)$$

G_j is zooplankton grazing rate in mmol m^{-3} d^{-1}, g is the maximum growth rate in d^{-1}, and $C_1 = P$, $C_2 = B$, and $C_3 = N_p$ are the three zooplankton food sources. The values p_j and p_k

are the preferences for a given food type, C_j and C_k, respectively with p_j and p_k defined by

$$p_j = \frac{\rho_j C_j}{\sum_{n=1}^{n=3} \rho_n C_n} \qquad p_k = \frac{\rho_k C_k}{\sum_{n=1}^{n=3} \rho_n C_n}$$

The preferences p_j will vary according to the relative proportions of the three food supplies thereby ensuring that the zooplankton concentrate their grazing on the most dominant food (FDM, 1990). The values of the ρ parameters are given in Table 2.

For bacterial uptake we have:

$$U_1 = \frac{V_b B N_d}{K_4 + S + N_d} \qquad (6)$$

$$U_2 = \frac{V_b B S}{K_4 + S + N_d}$$

with

$$S = \min(N_r, \eta N_d)$$

U is in mmol m^{-3} d^{-1} and V_B is the maximum bacterial growth rate in d^{-1}. The value η is the ratio of ammonium to dissolved organic nitrogen uptake that is required for bacteria to obtain enough nitrogen to be able to consume the carbon in dissolved organic matter. The above formulation ensures that bacterial uptake will always have an appropriate ratio of ammonium to dissolved organic nitrogen uptake, as explained by FDM(1990). Values for the parameters in these equations are given in Table 2.

Equations must also be specified for the $SMS(C_i)$ below z = 123 m. Physical processes, including vertical sinking of particulate organic nitrogen, will transport material out of the upper 123 m into deeper waters. The regeneration of this material needs to be parameterized. In our approach, all nonparticulate matter decays to ammonium and thence to nitrate. We thus have, for z > 123 m:

$$SMS(P, Z, B, N_d) = -\lambda(P, Z, B, N_d) \qquad (7)$$

$$SMS(N_r) = \lambda P + \lambda Z + \lambda B + \lambda N_d - \frac{\partial F(z)}{\partial z} - \lambda N_r$$

$$SMS(N_n) = \lambda N_r$$

$$N_p = 0$$

with λ given in Table 2. $F(z)$ is the flux of particulate material: thus we assume that the flux through one level that does not reach a deeper level was converted to ammonium in between. $F(z)$ is specified by an empirical function determined from Pacific Ocean sediment trap observations by Martin et al. [1987]:

$$F(z) = F(z')\left(\frac{z}{z'}\right)^{-v}$$

$z' = 123$ m, or the depth of the ocean floor, if that is shallower. The value v is given in Table 2. The downward flux of material at the base of the top six layers where the ecosystem equations are solved, i.e., the upper boundary condition at 123 m, is

$$F(z') = w_s N_p(z') - \int_{z'}^{0} \gamma_4 \mu_5 Z dz$$

The value of $F(z')$ is determined each time step from the production of particulate organic nitrogen in the upper 123 m during that time step. That is, sinking to a given depth and regeneration as ammonium at that depth happens instantaneously, which is why $N_p = 0$ below 123 m. Any particulate organic nitrogen that hits the bottom of the ocean is diffused back in as ammonium:

$$F(z_{bottom}) = D\frac{\partial N_r}{\partial z}$$

This equation serves as a bottom boundary condition for the ammonium balance equation.

The ecosystem equations (1) through (6) are solved in layers 1 to 6 of the model, down to a depth of 123 m (see Table 1). The behavior of the ecosystem model with higher vertical resolution has been examined with a one-dimensional version of the model. No significant differences were found (Evans, personal communication). The regeneration equations (7) are solved in layers 7 and below. No fluxes of the ecosystem components are permitted across the air-sea and sediment-water interfaces, except for the detrital flux which is returned as an ammonium flux, as explained above. The model does not contain a decay toward nutrient observations anywhere, including the two wall regions. It was found in preliminary simulations that damping toward observations made analysis of the results confusing because of the possibility of adding and removing nitrogen from the model through the damping terms. Our analysis is all produced at the end of a 3-year run, which is short enough that the interior region away from the walls is not adversely affected by the peculiar advection features in the regions adjacent to the walls.

Advection in the ecosystem equations is modeled by upstream differencing, whereas the GCM balance equations use centered differencing. We found that it was necessary to do this in order to avoid difficulties in the regions of strong lateral or vertical gradients which are frequently generated by the simulation. The centered differencing technique commonly generates unrealistic negative concentrations in such regions. Upstream differencing smooths sharp gradients, which is, in effect, an implicit diffusivity. The explicit lateral diffusivity is 10^7 cm^2 s^{-1}, and the vertical diffusivity is the Richardson number dependent diffusivity of Pacanowski and Philander [1981], with a background value of 0.1 cm^2 s^{-1}. It will be seen later that the vertical diffusivity plays only a minor role in the overall nutrient cycling.

The biological interaction terms can sometimes generate negative concentrations by overconsumption in a given time step. If such a negative concentration occurs, any biological source or sink terms dependent on that quantity are set to 0.

The model nitrate field is initialized with maps produced by Kawase and Sarmiento [1985] using Geosecs, TTO, Meteor 56/5, and Atlantis II 109 data. These data provide only modest resolution south of the Equator, with no stations against the African continent south of Dakar. The initial value for P is fixed at 0.14 mmol m^{-3} at the surface, decreasing exponentially with a scale length of 100 m with increasing depth. Z and B are fixed at 0.014 mmol m^{-3} at the surface, and N_r, N_d, and N_p at 0.1 mmol m^{-3}, all also decreasing exponentially with a scale length of 100 m.

2.3. Model Convergence

We analyze the model results after the ecosystem model components have recovered from the perturbation caused by the inconsistency between the initial conditions and the model, but before the longer time scales of the evolution of the nutrient field in the thermocline and deep ocean can come into play. Ideally we would analyze the model after a dynamical equilibrium of the annual cycle is achieved, i.e., when the annual cycle repeated itself exactly from one year to the next.

Such an equilibrium would require much longer computer runs in order to bring the deep ocean into equilibrium, and greater attention to the way that we deal with regeneration. These are tasks which we are approaching with a different modeling strategy.

Figure 2 shows the evolution of the ecosystem components in the upper 123 m of the model during the first 3 years of the simulation. They all have an increasing trend which is most

evident in nitrate and ammonium. However, the pattern of the annual cycle is set before the end of the first year, even for nitrate and ammonium. Figure 3 shows the annual rate of change of phytoplankton, nitrate, and total nitrogen integrated over the upper six model layers. The analysis of Figure 3 shows that the initial perturbation in phytoplankton lasts two years, after which the annual rate of change drops smoothly and rapidly (Figure 3a). This behavior is typical of all
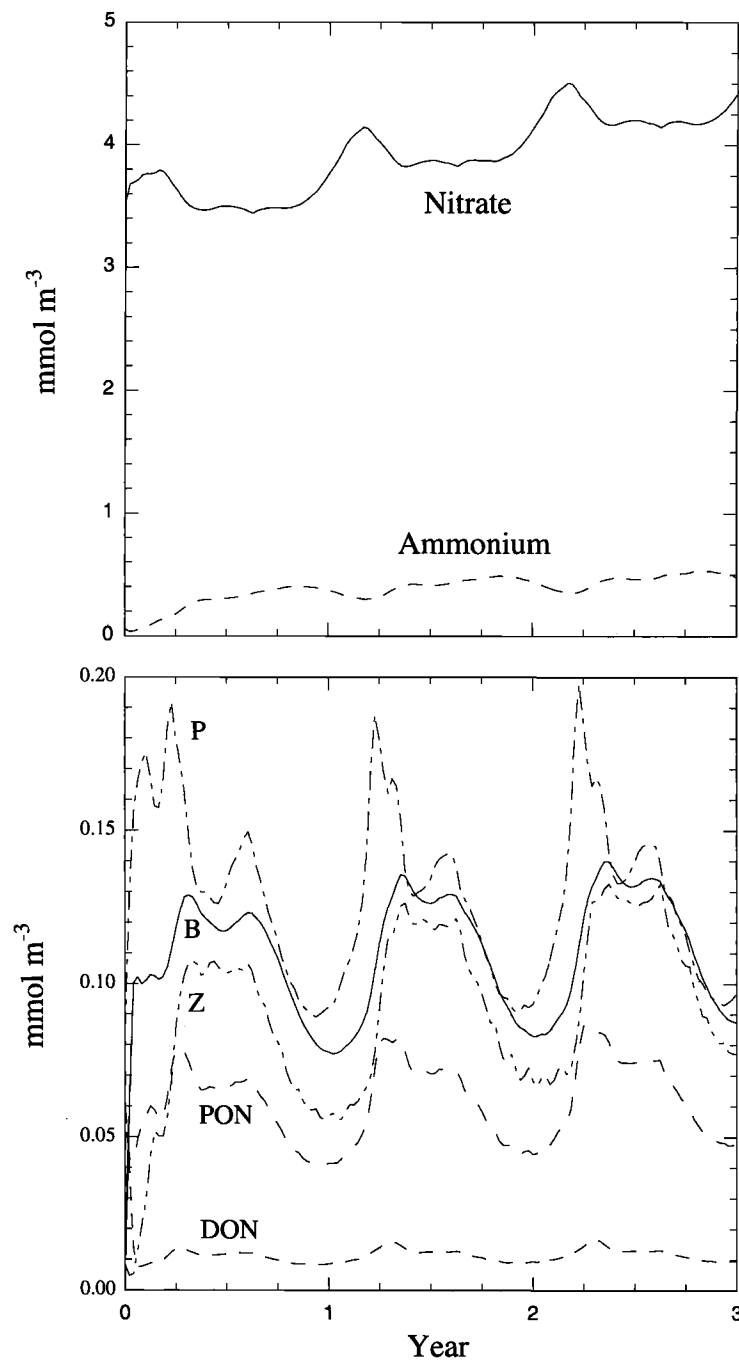
Fig. 2. Weekly mean concentrations of the ecosystem components for the first 3 years of the simulation.

ecosystem model components except ammonium and nitrate, both of which follow the pattern of nitrate shown in Figure 3b, with a milder initial perturbation, and a slower convergence. All our analysis is done during the third year of
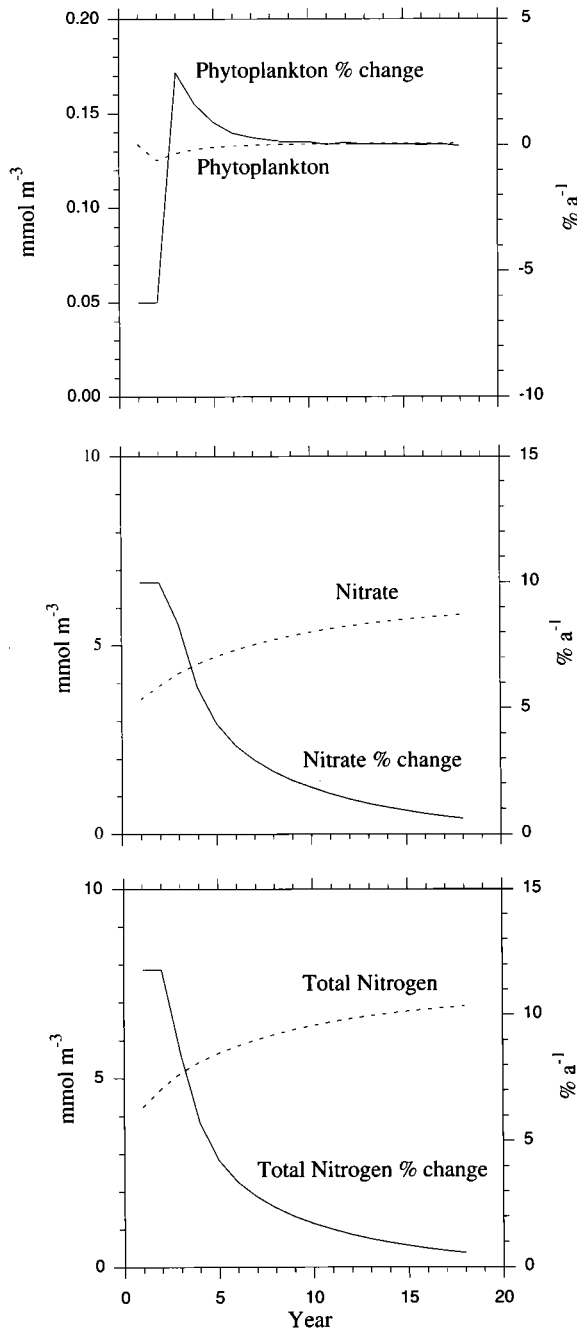

Fig. 3. Annual mean concentrations of (a) phytoplankton, (b) nitrate, and (c) total nitrogen (the sum of the concentration of all seven components of the ecosystem model) in the upper 123 m of the model over a 19-year simulation. Also shown is the percent change per year.

the simulation, after phytoplankton and the other ecosystem components have begun their smooth convergence.

The 19-year trend in total nitrogen shown in Figure 3c is driven primarily by nitrate and ammonium, which account for 91.8% of the total in the year 3 annual average. As the amount of nitrogen in the upper 123 m increases, the biomass, dissolved organic nitrogen and particulate organic nitrogen increase only modestly. Most of the nitrogen stays as nitrate or gets converted to ammonium by the ecosystem interactions

Figure 4 shows a map of the change in nitrate content that occurs over the full model domain from 30°S to 68°N, between the beginning and end of the third year of the simulation. The largest changes occur in the region south of the Equator where the circulation model has considerable upwelling due to the way we deal with the presence of a wall there. Because of this problem, which is compounded by the fact that the data with which we initialized the simulation are sparse in this region, we believe that the simulation in this area is flawed. The time rate of change in the rest of the model is much smaller. The pattern in the rest of the model is also strongly driven by the pattern of the circulation. Interestingly, there is a tendency for upwelling regions around the subtropical gyre to be losing nitrogen, whereas the downwelling central portion of the gyre is slowly gaining nitrogen. The lateral transport divergence from upwelling regions, and the convergence in downwelling regions, exceeds the vertical transport in both locations during year 3. If the model were allowed to converge to a solution, the lateral transport divergence would equal the vertical.

3. RESULTS

This section gives an overview of the flow of nitrogen from its transport into the surface in the dissolved inorganic form, through to its export from the surface ocean as organic matter
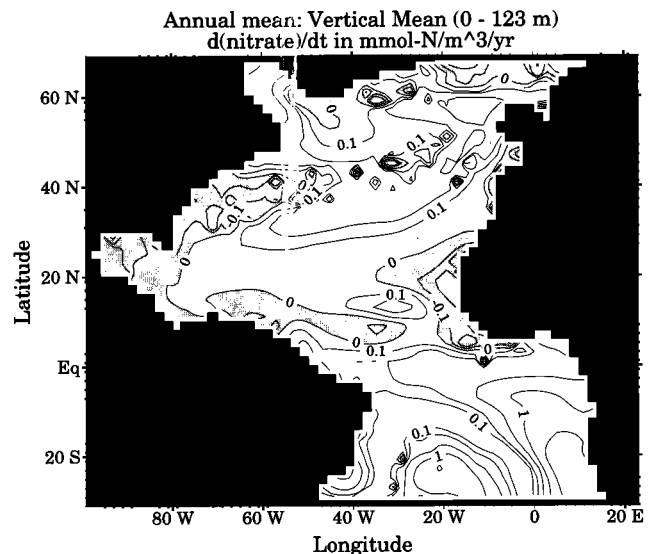

Annual mean: Vertical Mean (0 - 123 m) d(nitrate)/dt in mmol-N/m^3/yr

Fig. 4. Map of the change in nitrate concentration during year 3 of the simulation. Contour interval is 0, ±0.1, ±0.2, ±0.5, ±1.0, ±2.0, etc.

The analysis focusses on the vertically integrated behavior of the model over the entire euphotic zone (the top six layers equal 0 to 123 m), and in the upper two layers of the model used in making the comparison to satellite chlorophyll data in the discussion section (0 to 23 m). A companion paper discusses the vertical structure of the model results [Fasham et al., this isssue]. Although the model covers the regions from 30°S to 68°N, results are presented only for the region 20°S to 60°N, away from the direct influence of the walls.

3.1. Nitrate Transport

Figure 5 shows the annual mean nitrogen balance of the upper 123 m during year 3. The net vertical input of nitrate to the upper 123 m is 64% by upwelling and 29% by convective overturning, with a relatively minor 7% contribution due to

vertical mixing. Horizontal exchange with the wall regions removes a small amount of nitrate equivalent to 3% of the total vertical input. The strong influence of upwelling shows clearly in the close correlation of a map of the vertical supply of nitrate across 123 m (Figure 6a) with the pattern of upwelling at 123 m (Figure 7a). The only major area where this correlation breaks down is in a broad southwest-northeast trending band in the northern portion of the subtropical gyre centered on a line from ~35°N to ~55°N. Here the model predicts a positive supply of nitrate in a region where the vertical velocity is downward. The physical mechanism for this positive supply is convective overturning, which is strong enough at 123 m in this area to overcome the influence of downwelling (Figure 7b).

Horizontal nitrate transport over the 0 to 123 m depth range (Figure 6b) tends to be a mirror image of the vertical transport
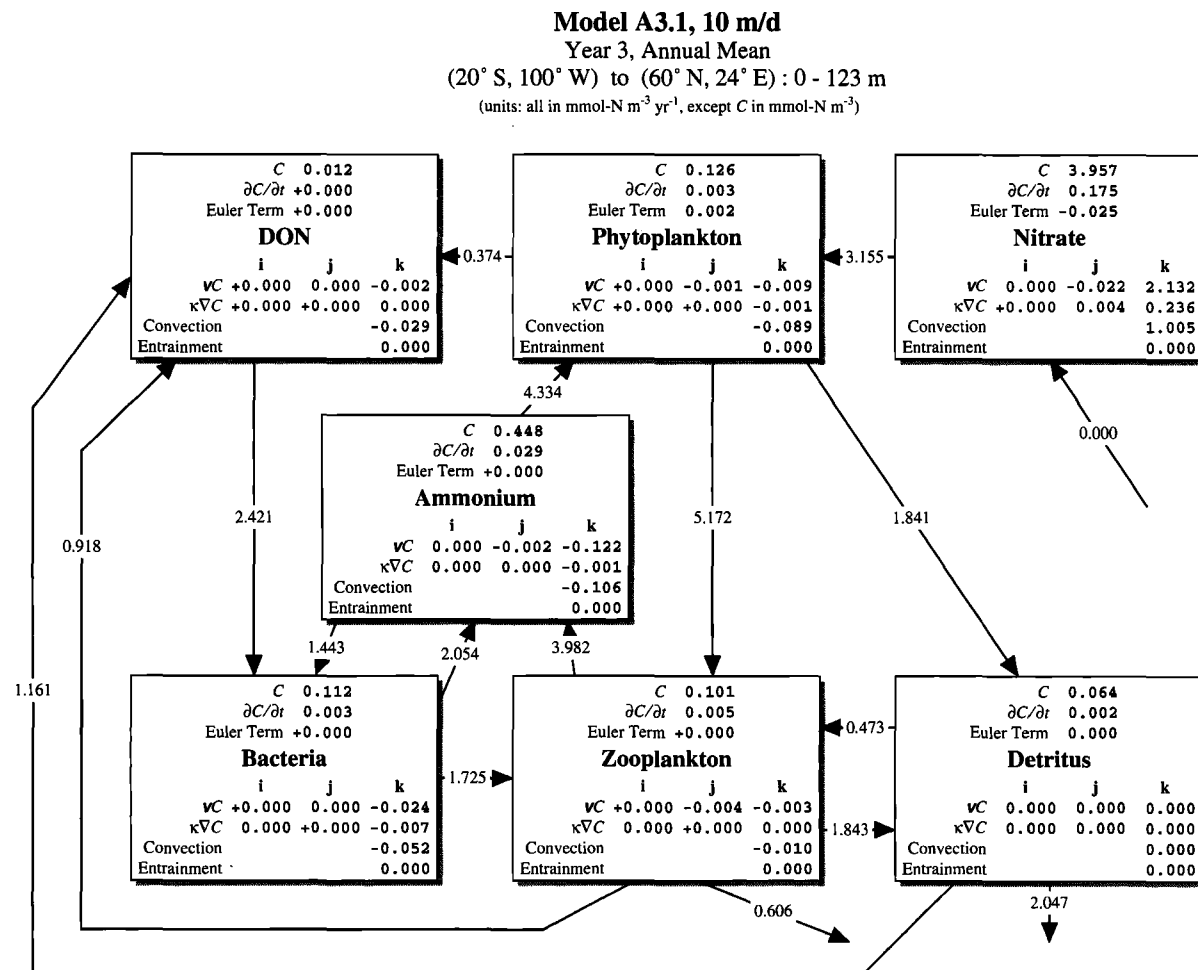

Fig. 5. The annual mean contribution over the whole model of all terms in the ecosystem model in year 3 of the simulation. See Figure 1 and the text for a more detailed description of the biological interaction terms that are represented. The lower half of each box shows the physical interaction terms, with velocity at the top, diffusion in the middle, and convection at the bottom. Values i, j, and k, represent the x, y, and z directions, respectively. The time rate of change terms ($\partial C/\partial t$ and the so-called Euler term, which represents a special time step that is required by the finite differencing technique which is used) are a measure of the extent of disequilibrium of the model. They would eventually reach 0 if the model were run to steady state.
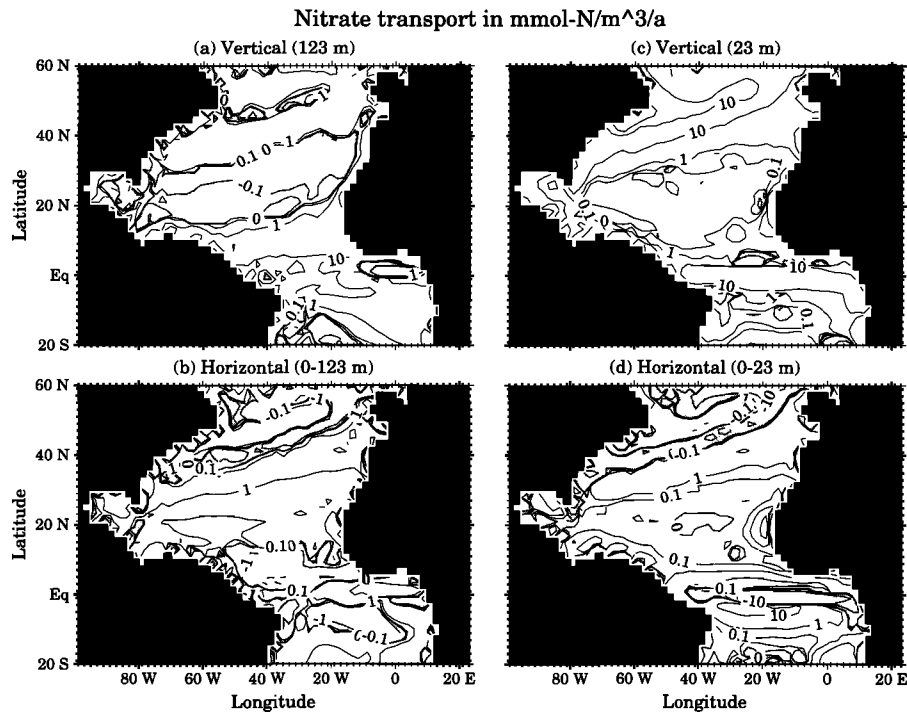
Nitrate transport in mmol-N/m^3/a

Fig. 6. (a) and (b) Vertical and horizontal annual mean supply of nitrate to the top 123 m of the model. (c) and (d) Vertical and horizontal annual mean nitrate supply to the upper 23 m of the model. The contour interval is 0, ±0.1, and ±1 mmol-N m-2 d-1. The stippling indicates removal of nitrate.

at 123 m. This is because the divergent horizontal flow associated with upwelling generally carries high nutrient upwelled water to convergent regions of nutrient poor downwelling water. However, the regions of deep convection shown in Figure 7b interfere with this pattern, sometimes giving rise to areas such as the northern part of the central portion of the subtropical gyre, where both horizontal and vertical transport are of the same sign.

The overall pattern of upwelling and downwelling is determined primarily by the Ekman transport at the surface. Divergent Ekman flow in the subpolar gyre and at the equator drives upwelling. Convergent Ekman flow in the subtropical gyre drives downwelling. The near-surface (23 m) vertical velocity pattern (Figure 7c) determined by this Ekman transport survives with only minor modifications to 123 m (Figure 7a) except for the disappearance of strong downwelling just north of the equator. This downwelling feature is associated with a shallow recirculation cell whose existence has been noted before in connection with studies of the North Atlantic heat budget [Hastenrath, 1977; Sarmiento, 1986].

The large-scale pattern of subtropical gyre downwelling at 123 m (Figure 7a) extends to the north of the band of deep convection in the model (Figure 7b). As a result, there is a narrow southwest-northeast trending tongue of negative vertical supply projecting out from the North American continent at approximately 45°N (Figure 6a). The absence of deep convection in this tongue of negative vertical nutrient supply is not supported by data-based estimates of mixed layer

thickness, which show deep mixed layers occuring throughout the region (Figure 8). Sarmiento [1986] points out that this lack of convection is a result of the Gulf Stream being too far north in the model. Since surface waters off the North American coast are less dense than waters found in the Gulf Stream, the presence of the Gulf Stream near the shore stabilizes the water column to convection. Similarly, the dense waters of the Labrador Current, which otherwise would flow south along the continent, are forced out into interior regions where the waters have lower surface density, thus tending to stabilize the water column to convective overturning in the interior. The large horizontal supply of nutrients to this region (Figure 6b) compensates for the lack of vertical input.

3.2. Nitrogen in the Food Chain

Nitrate enters the food chain by photosynthetic uptake and is removed from the surface primarily as particulate organic matter formed by phytoplankton mortality and zooplankton egestion and mortality (84%), with a significant (15%) contribution from direct transport of phyptoplankton, zooplankton, bacteria, ammonium, and dissolved organic nitrogen (see balances in Figure 5). 1.3% of the nitrate goes into an increase in the concentration of the ecosystem components, primarily ammonium, between the beginning and end of the year. Figure 9 shows the primary production, and nitrate and ammonium uptake by phytoplankton in the model
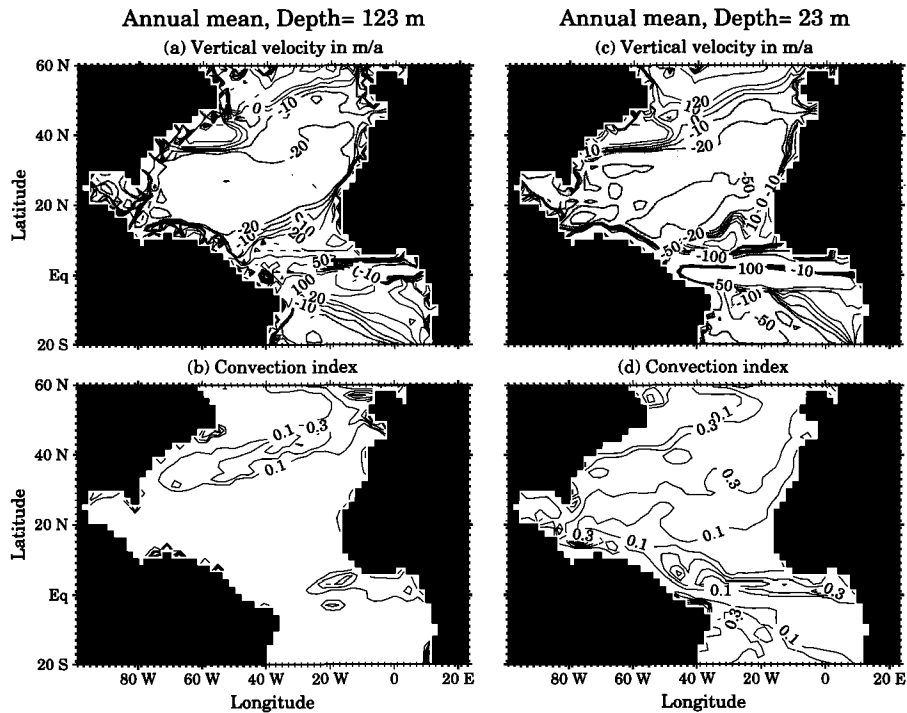
Fig. 7. Annual mean vertical velocity and convection index at a depth of (a) and (b) 123 m and (c) and (d), 23 m, respectively. The convection index is defined as the fraction of time that the model is convecting at a given location.

The development and subsequent collapse of the spring bloom in the subpolar and northern half of the subtropical gyres is evident in Figure 10a. A comparison of Figures 9b and 10a with 9d shows that direct uptake of nitrate (new production) fuels the early part of the bloom. Later on, however, the increase in ammonium concentration (Figure 10d) leads to inhibition of nitrate uptake and its replacement by ammonium uptake (Figure 9f). The ammonium is produced mainly by zooplankton, with a small net production by bacteria (see balances in Figure 6). Zooplankton and bacteria do not develop until later in the bloom (see standing crops in Figures 10c and 10e, respectively, and productions in Figures 11b and 11c). The sedimentation (sinking of particulate organic nitrogen) is not limited to the period of nitrate uptake but rather continues throughout the entire time when the phytoplankton production is occurring (Figure 11d). The annual average f ratio (ratio of new production resulting from nitrate uptake to the sum of new production and regenerated production resulting from ammonium uptake) is 0.43, but Figure 12 shows the high values during the early part of the spring bloom (the time when new production is dominant) and abrupt plunge afterward (when regenerated production is dominant) that would be expected from the above results. The f ratio unexpectedly continues to be low through the winter. The cause is residual ammonium produced earlier in the year.

The geographic pattern of new production (Figure 9c) must, of necessity, be directly correlated with the supply of nitrate by transport (Figure 6), since, in a steady state, these two quantities will equal each other. However, the geographical

pattern of the primary production (Figure 9a) differs somewhat from that of the new production because of the formation and lateral transport of ammonium, as a result of which the consumption of ammonium occurs over a wider area than nitrate. This is particularly evident in the equatorial and coastal upwelling regions of the low latitudes (Figure 9e).

3.3. Control of Surface Nitrate Concentration

We now proceed to an analysis of results in the upper 23 m. Figure 13 shows that nitrate supply to the upper 23 m is low throughout the model except in the high latitudes during winter, and in the equatorial region. As would be expected, surface nitrate concentrations are generally low in the same regions and at the same time when transport is low (Figure 14). However, the correlation between high transport and elevated nutrient concentrations is complex. Nitrate at the equator never goes much above 2 mmol m^{-3} in the zonal mean, (Figure 14), despite having the highest transports in the model (Figure 13), whereas the wintertime high latitudes, despite having a smaller nitrate supply than the equatorial region, go above 10 mmol m^{-3}. This results from the fact that the period of enhanced nutrient supply in the high latitudes occurs when light levels are low due to the low wintertime sun angle (Figure 15b) and the presence of deep mixed layers (Figure 8).

Perhaps the most interesting outcome of the model in the surface waters of the high latitudes is that nitrate remains well above ~1 mmol m^{-3} in some areas during the summer, despite

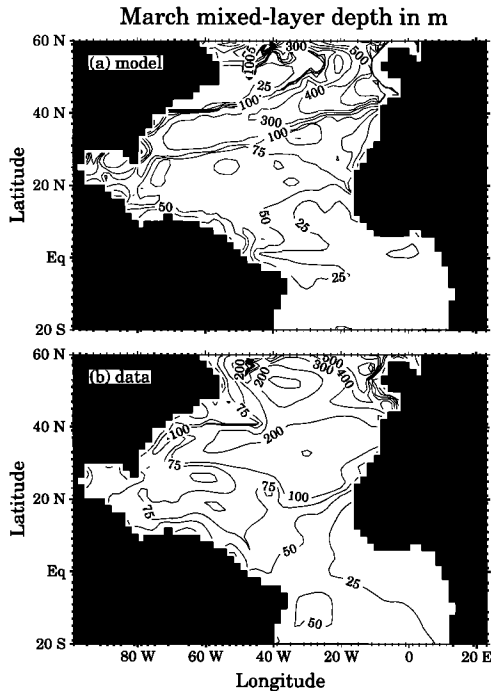## March mixed-layer depth in m

Fig. 8. (Upper panel) Mixed layer depth calculated by the model and (lower panel) observational based estimate of Levitus [1982]. Note the deep trough in the northern half of the subtropical gyre of the model which is not supported by the observations. Figure taken from Sarmiento [1986].

the fact that nitrate supply is small and light supply high. Fasham et al. [this issue] discuss the relevant processes for Ocean Weathership Station (OWS) India. We define potential nitrate limitation as the nitrate limitation term Q_1 defined by (3), divided by $e^{-\psi N_r}$, the ammonium inhibition. A comparison of the nitrate limitation term with the potential nitrate limitation (Figure 16), shows that an immediate cause of low nitrate uptake in the high latitudes during the late spring, summer and early fall months is ammonium inhibition. The importance of ammonium can also be readily discerned in the plots of Q_1 and the ammonium limitation term, Q_2, (Figure 15c and d), which show that ammonium is by far the preferred nutrient for phytoplankton growth during the late spring, summer, and early fall months. As pointed out above, the main source of ammonium is zooplankton.

On the other hand, ammonium inhibition cannot be the only factor, inasmuch as it is possible, in principle, for the phytoplankton population to expand to the point where it depletes both ammonium and nitrate. For example, nitrate and ammonium are abundant in the northern half of the subtropical gyre between approximately 20°N and 35°N to 40°N during the winter, but depleted in the late spring, summer, and early fall. To understand what prevents the phytoplankton population from expanding sufficiently to the north of this requires examining what controls the phytoplankton population.

Figure 17 shows the P normalized terms of the phytoplankton balance equation,

$$(1/P)(dP/dt) = [(1-\gamma_1)\mu_P - \mu_m] - \mu_g + \mu_t$$

which is what Fasham et al. [this issue] use to explain the processes at OWS India. The term $(1/P)(dP/dt)$ is the specific rate of change of phytoplankton. The value μ_P is the specific phytoplankton growth rate, γ_1 the fraction of phytoplankton growth exuded as dissolved organic nitrogen, and μ_m the specific mortality rate, 0.04 d^{-1}. The terms grouped inside the brackets sum up to give the specific "net" phytoplankton growth rate. The value μ_g is the specific loss rate due to grazing, and μ_t is the specific gain or loss rate due to all physical processes. Figure 17b shows that transport of phytoplankton is negligible. Thus the primary terms contributing to the change in P with time (Figure 17d) are the specific net growth rate (Figure 17a) and the specific zooplankton grazing term (Figure 17b). The normalized net production is positive throughout the year except during the winter time in high latitudes. Figure 17d shows that this net production leads to a rapid expansion of the phytoplankton population in the late winter and early spring. This expansion is cut off and forced to change sign for a period of 2 to 3 weeks by zooplankton grazing. Thereafter the overall growth rate of phytoplankton continues at a small positive number on the average because of grazing by zooplankton.

An additional factor in the elevated summer nitrate concentrations of the high latitudes is continued input of nutrients noticeable in the highest latitudes of Figure 13a and analyzed in detail at OWS India by M. J. R. Fahsam et al. (manuscript in preparation, 1993). Although the spring bloom depletes nitrate at OWS India to as low as 0.2 mmol m^{-3} in May, it rises thereafter to just over 1.5 mmol m^{-3}. The influence of a continuous nutrient supply such as this on ecosystem behavior is most readily understood by an analysis of the equatorial region, where the supply of nutrients and light is nearly constant throughout the year, so that the model can be considered to be approximately in steady state.

Because it is approximately at steady state, the concentration of surface nitrate in the equatorial region is fixed at the level required for phytoplankton to take it up at the same rate it is being supplied. The half-saturation constant for nitrate uptake is 0.5 mmol m^{-3}. Thus nitrate concentration is not required to be very high in order to have an efficient ecosystem throughput (Figure 14). If the supply of nitrate were too high, i.e., if the phytoplankton population (the maximum concentration of which is limited by zooplankton grazing) were insufficient to take up nitrate at the rate it is supplied, the model would be forced to adjust so as to slow the rate of supply. This would be accomplished by an increase in the surface nitrate concentration to the point where it would be comparable to that of the subsurface waters that are supplying the surface. This does not occur at the Equator in the model during the winter when the nitrate supply is lower, but it does occur in the high latitudes during the winter, and to a lesser extent at the Equator during the summer (Figure 14). The concepts of a phytoplankton uptake dominated system versus a transport dominated system are further explored in the discussion section.

4. DISCUSSION

The discussion focusses on three major topics. The first is a comparison of model results with satellite coastal zone color scanner (CZCS) observations, with the aim of examining the
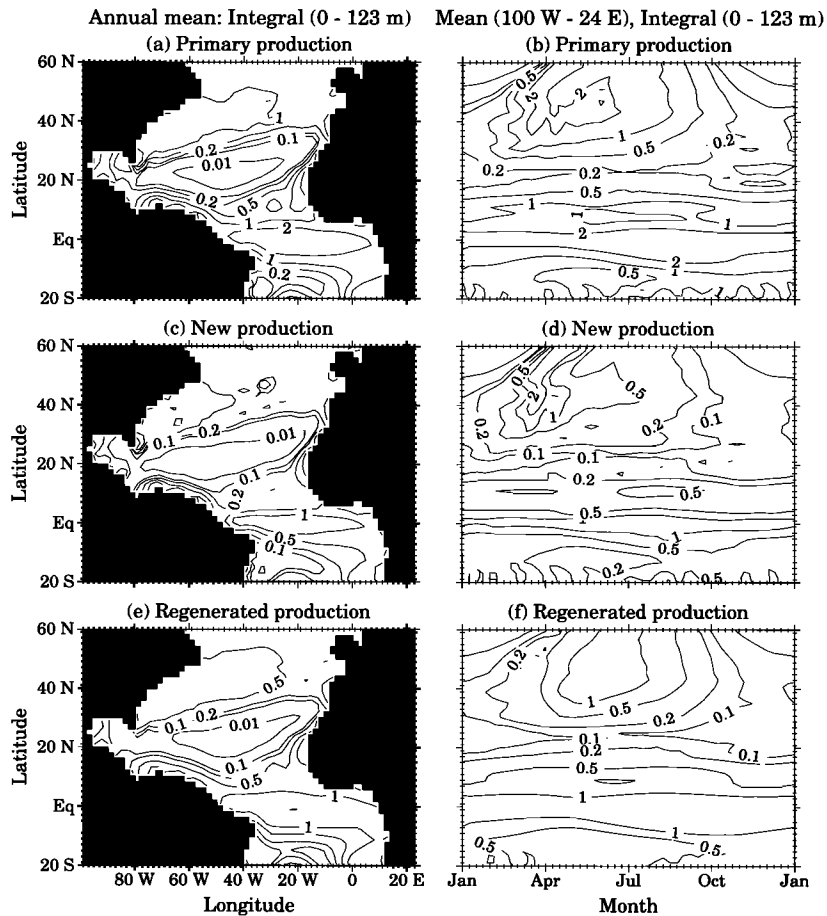
Phytoplankton production in mol-N/m^2/a

Fig. 9. (a) and (b) Primary production, (c) and (d) uptake of nitrate by phytoplankton, and (e) and (f) ammonium uptake by phytoplankton. The contour interval is 0.01, 0.1, 0.2, 0.5, 1.0, and 2.0 mol m^{-2} yr^{-1}. The left-hand panels show annual means over the top 123 m. The right-hand panels show zonal integrals over the top 123 m as a function of latitude and time. The development of the spring bloom shows as contours which slope upward to the right (e.g., in Figures b and d), as the bloom begins first at low latitudes then progresses gradually to higher latitudes. The model bloom develops about a month too early in the model, as discussed in the text.

validity of the model and identifying areas of needed model improvement. The second and third sections address two of the major issues raised in the introduction of the paper, namely, what controls the surface nutrient concentration, and how is the new production related to the primary production? The third section also discusses the magnitude of the new production.

The introduction raised a question about the form in which organic matter leaves the surface. As pointed out earlier, 85% of the nitrogen in our model is transported out as particulate organic nitrogen, with the remainder being transported out in the form of phytoplankton, zooplankton, bacteria, ammonium, and dissolved organic nitrogen. However, our model in its present form intentionally left out production and consumption of less labile dissolved organic matter as suggested by Toggweiler [1989], Bacastow and Maier-Reimer [1991], and

Najjar et al. [1992], since including it would have required costly model runs of order 1000 years to converge to a meaningful solution. Thus our model does not provide a basis for analyzing the form in which organic matter leaves the surface.

4.1. Comparison With Chlorophyll Observations

The model results can be compared with a variety of observations. This paper concentrates on the CZCS chlorphyll estimates because of the good spatial and temporal coverage of these data. A companion paper examines more detailed aspects of the model by comparison with observations at Bermuda Station "S" and Ocean Weathership Station (OWS) India [Fasham et al., this issue]. A problem with our effort is that there is a dearth of suitable data from which annual means
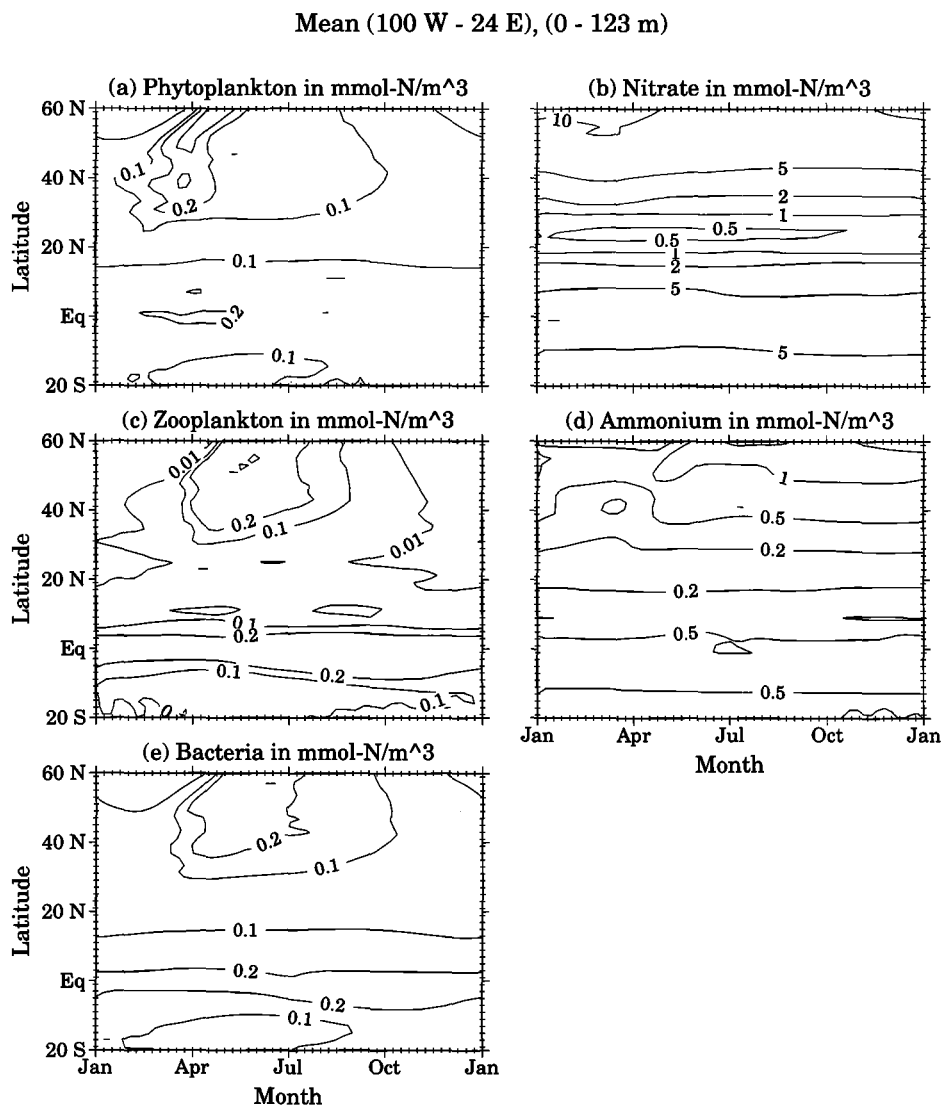
Mean (100 W - 24 E), (0 - 123 m)

Fig. 10. Zonal mean standing crops of phytoplankton, nitrate, zooplankton, ammonium, and bacteria in the upper 123 m of the model. The contour interval in all three figures is 0.01, 0.1, 0.2, 0.5, 1, 2, 5 and 10 mmol-N m^{-3}.

or annual cycles can be determined except at just a few sites like Bermuda and OWS India.

Plate 1 shows annual mean pigment concentrations estimated from phytoplankton nitrogen concentrations predicted by our model in the upper two layers (23 m depth), compared with satellite CZCS based estimates obtained from Esaias et al. [1986] and Feldman et al. [1989]. The model nitrogen concentration was converted to chlorophyll using a nominal g chlorophyll to mol nitrogen ratio of 1.59, which corresponds to a chlorophyll to carbon mass ratio of 1:50 and a C:N mole ratio of 6.625. The CZCS measures light backscattered from the upper water column with a mean attenuation depth scale of the order of 10 m [Gordon et al., 1982]. The upper two layers of our model down to 23 m are generally well mixed, thus we concluded that a reasonable

comparison with CZCS observations could be made with the mean properties of the upper two layers of the model.

The emphasis of the discussion that follows is to identify areas of disagreement between model and observations since this is how one learns the most about how to improve the model. First, however, it is important to point out that the overall pattern of the model predicted annual mean chlorophyll agrees quite well with the CZCS data (Plate 1). This agreement is particularly impressive in view of the use of a single rather simple ecosystem model calibrated with data at only one location, Bermuda Station "S". The only sources of variability in the model are the physical transport, whose primary direct influence is on the supply of nitrate; light, which varies with latitude, but is also strongly influenced by the depth of mixing in the model; and temperature, which

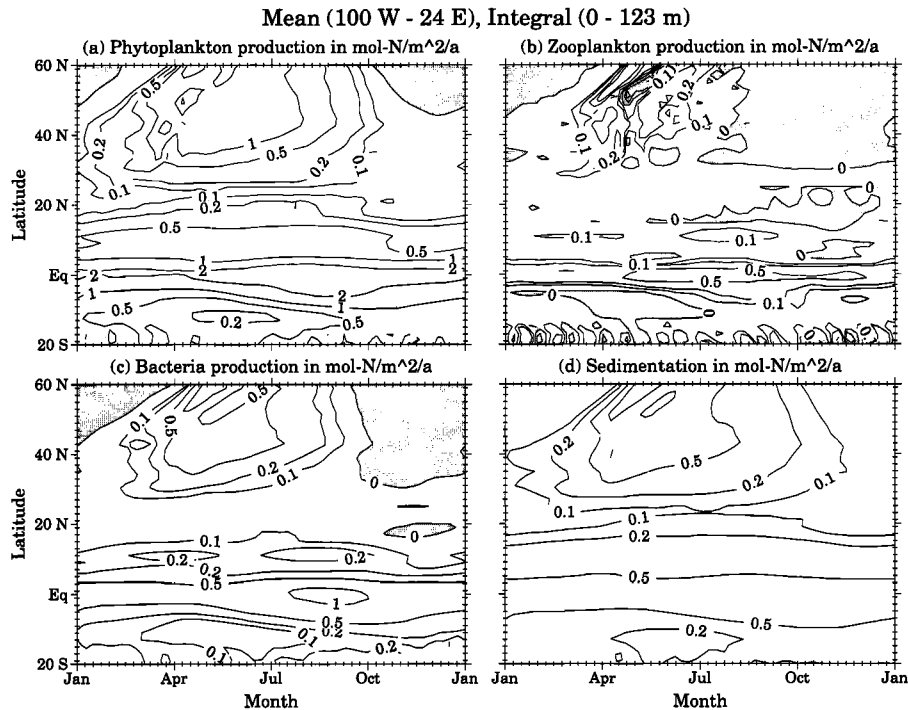Mean (100 W - 24 E), Integral (0 - 123 m)

Fig. 11. Zonal mean Phytoplankton, zooplankton, and bacterial production, and sedimentation in the upper 123 m of the model. The contour interval is 0, ±0.1, ±0.2, ±0.5, ±1, ±2, ±5, and ±10 mmol m^{-3} yr^{-1}.

affects the phytoplankton maximum growth rate V_p. The excellent agreement between model and observations in terms of the basinwide pattern, and the amplitude of chlorophyll concentration when the supply rate is high in spring, underscores the importance of the physical environment in determining the behavior of ocean biology. The strong physical driving of the spatial patterns of the lower trophic levels has also been observed in the regional studies of Wroblewski [1977], Walsh and McRoy [1986], Hofmann [1988], and Walsh et al. [1988].

The model shows high pigment concentrations where the supply rate of nitrate is high, as in the subpolar and northern subtropical gyres, and low concentrations in regions of low nitrate supply rate such as the southern half of the subtropical gyre (Figure 6 and Plate 1a). These patterns can be seen in the satellite observations as well (Plate 1b). Most of the high pigment coastal upwelling zones observed in the CZCS data off the northeastern coast of South America and off of Africa have counterparts in the model, albeit rather weak ones. The major exception is in the Gulf of Guinea where Figure 7c shows that the model predicts downwelling in a region where the expectation from the satellite observations is that there should be a significant upward supply of nutrients. Another area of major disagreement between the model and observations is in the interior of the equatorial region, to be discussed in more detail below.

The seasonal CZCS data shows a strong spring bloom in the subpolar gyre with continued high pigment levels into the fall, and even (in some regions) during the winter (Plate 2).

However, the CZCS results cannot be trusted for the months of September or October to December for latitudes greater than approximately 40°N, during which time they appear to be higher than observations by a very substantial amount [Yoder et al., 1993]. The model pigment concentrations also show a spring bloom, but the chlorophyll concentrations are much higher than those obtained from the CZCS observations, with concentrations subsequently dropping earlier than the observations and reaching levels that are much lower than the observations during the summer, fall, and winter. The difference in the timing and amplitude of the spring bloom between the model and CZCS observations is dramatically illustrated by a plot of the ratio of zonal mean model to CZCS chlorophyll (Figure 18), although it should be kept in mind that this plot tends to obscure the excellent agreement between the model and CZCS observations in the central region of the model. Fasham et al. [this issue] discuss this problems in some detail in their comparison of the model predictions to the detailed observations at OWS India [cf. Fasham, 1993]. They suggest that a reduction in zooplankton mortality during times of low food supply in the winter may be required. This would enable the zooplankton to expand earlier in response to the spring bloom, thus preventing the higher phytoplankton accumulation predicted by the present model. The inclusion of a micro grazer component would help as well, because the growth rates of micro grazers such as protozoan ciliates are more closely coupled to the growth rate of the phytoplankton. One of the major lessons of the Joint Global Ocean Flux Study (JGOFS) North Atlantic Bloom Experiment was the
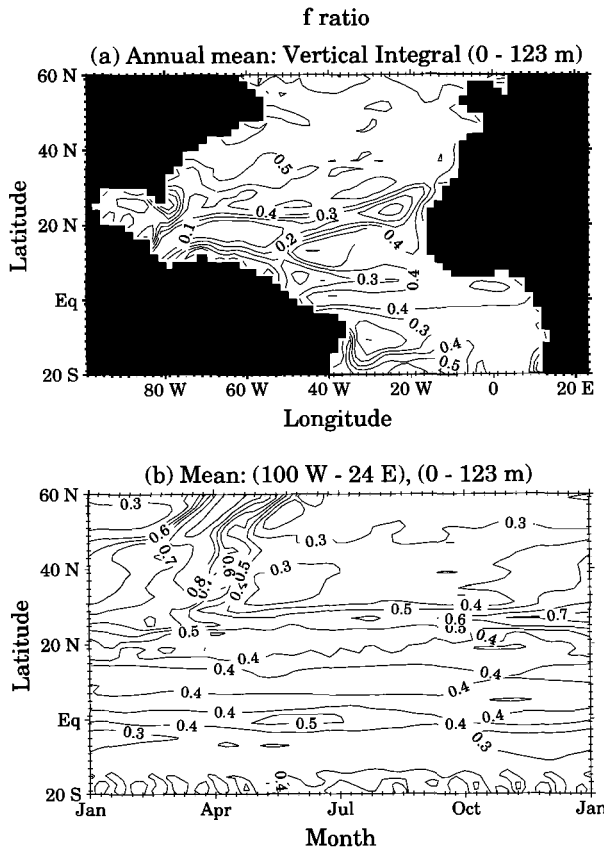
f ratio

(a) Annual mean: Vertical Integral (0 - 123 m)

(b) Mean: (100 W - 24 E), (0 - 123 m)

Fig. 12. The f ratio (new production over the sum of new and regenerated production) predicted in the upper 123 m of the model. Note in the upper panel that the annual mean f ratio is high in regions of high-nitrate supply and high production, and low in regions, such as the southern half of the subtropical gyre, of low-nitrate supply and low production. The lower panel shows large seasonal variations of the f ratio which are discussed in the text. The contour interval is 0.1

Total nitrate transport in mmol-N/m^3/a
Mean: (100 W - 24 E), (0 - 23 m)

Fig. 13. Time latitude plot of the zonal mean nitrate supply rate to the upper 23 m. Contour interval is 0.02 mmol m^{-3} d^{-1}

Nitrate in mmol-N/m^3
Mean: (100 W - 24 E), (0 - 23 m)

Fig. 14. Time latitude plot of the zonal mean nitrate content Contour interval is 0.01, 0.1, 0.2, 0.5, 1, 2, 5, and 10 mmol m^{-3}.

importance of fast grazers, even in the bloom season [cf. Longhurst, 1991].

Fasham et al.'s [this issue] OWS India analysis also points towards a major problem with the model prediction of temperature during the summertime. Warming does not penetrate deeply enough into the seasonal thermocline in the model. A more realistic simulation allowing heat penetration into the thermocline, and thus reducing the vertical stability, might give a higher supply of nutrients to the surface. Preliminary simulations show that much of the seasonal thermocline warming is a result of the deep penetration of short wave solar radiation (R. C. Pacanowski, personal communication, 1992). This feature is not included in the present version of the model.

The northern half of the subtropical gyre has high pigment levels in the late winter and spring which are not supported by the observations (Plate 2 and Figures 18). Part of the reason for this is the simulation of the winter mixed layer in the
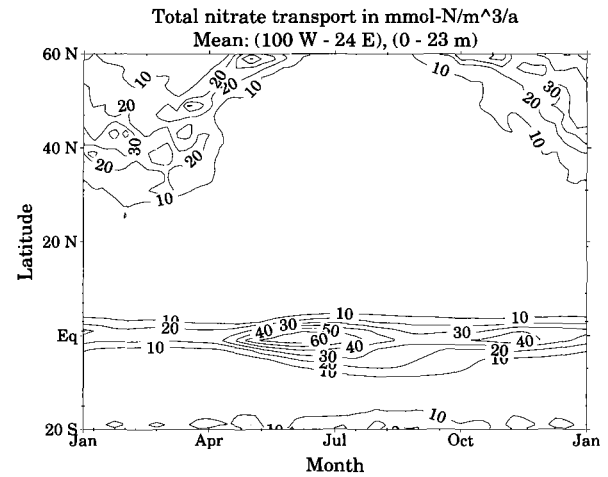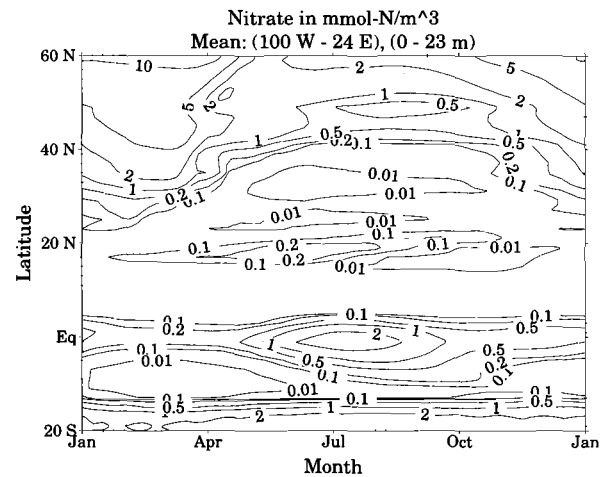
model. As Figure 8 shows, the model has a very deep mixed layer trough in the northern half of the subtropical gyre that is not supported by the observations. This trough of deep mixing provides high nutrient content to fuel a strong bloom A simulation using the less deep observationally based Levitus [1982] mixed layer (Figure 8b) does a better job in this region, including giving a better timing of the spring bloom (data not shown). The bloom is about a month early in our model due to a too early shallowing of the mixed layer. Levitus's data have a later shallowing.

The phytoplankton concentrations predicted by the model in the southern half of the subtropical gyre are almost an order of magnitude lower than observed concentrations. We have seen above that in this region of the model nitrate is supplied laterally. Vertical transport, which is dominated by downwelling, removes nitrate. The comparison of model
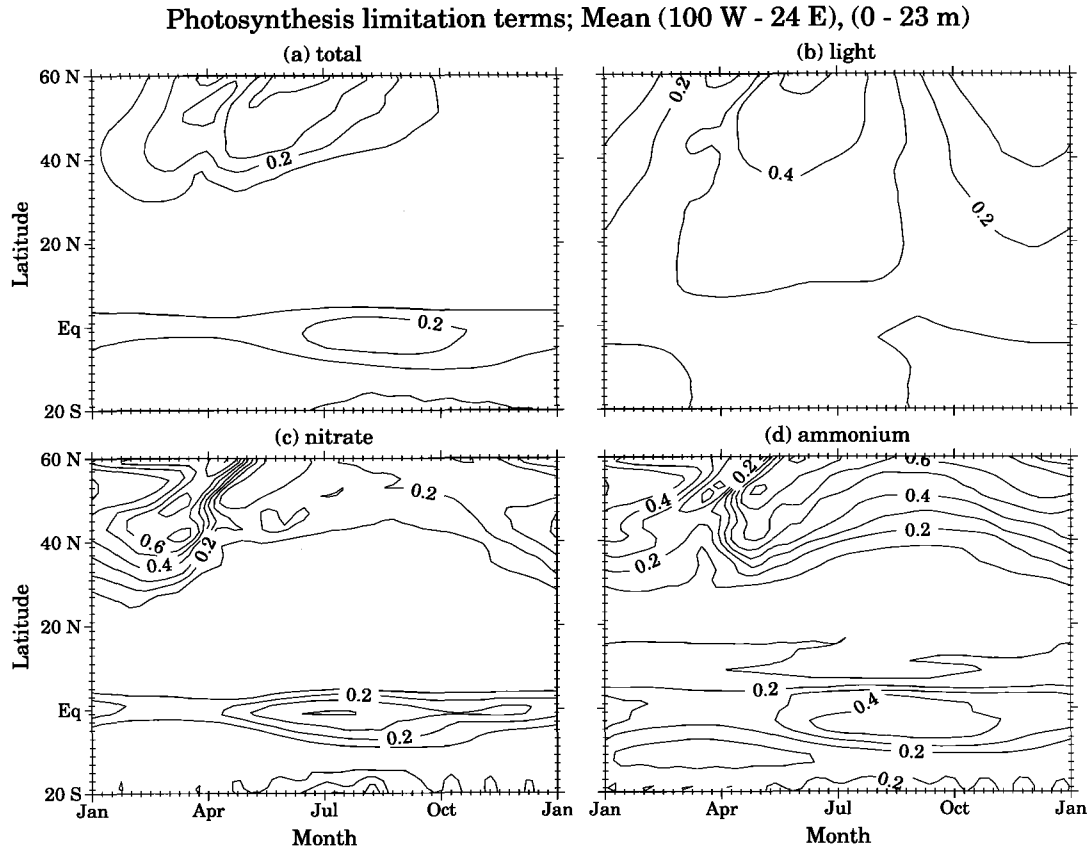
Photosynthesis limitation terms; Mean (100 W - 24 E), (0 - 23 m)

Fig. 15. Upper 23 m time latitude zonal mean plots of (a) $(\bar{J}(z,t)/V_p)(Q_1(N_n,N_r)+Q_2(N_r))$, (b) $(\bar{J}(z,t)/V_p)$ (c) $Q_1(N_n,N_r)$, and (d) $Q_2(N_r)$ These terms are defined by (2), (3) and (4). Contour interval of all plots is 0.1.

predicted surface heat flux with observations shown in Figure 19 (taken from Sarmiento [1986]) shows that the flux of heat into the ocean predicted by the model is lower than observations in this region. In order to increase the heat flux, the supply rate of cold water from the thermocline to the surface must be increased so as to enhance the air-sea temperature gradient. Such an increase in thermocline water supply rate might also increase the supply of nutrients.

The equatorial region of the model shows pigment concentrations that are higher than observations in the interior, and generally lower off the coast of Africa. The high model heat flux along the model equator (see Figure 19) suggests that supply of cold, nutrient rich thermocline waters may be too high. R. C. Pacanowski (personal communication, 1992) has shown that penetration of short wave radiation does not have a significant impact on the simulation in this region. We have explored another solution based on the suggestion by Harrison [1989] that the Hellerman and Rosenstein [1983] wind stresses we use appear to be about 30% too high at the equator. A reduction of 30% in the wind stress decreased the pigment concentrations at the equator dramatically, but the basic pattern of highest concentrations in the middle of the gyre and low concentrations off Africa remained. Thus a possible explanation for the problems we are encountering at the equator is that the interior wind stresses are indeed weaker, and

that the pattern along the African coast is significantly different.

4.2. Control of Surface Nitrate Concentration

The tendency of ocean circulation and mixing is to drive nutrients from areas of high to low concentration, to continually force surface nutrient concentrations toward deep concentrations. The low concentrations observed in the surface ocean (Figure 20a) are thus a clear indication of the importance of the biological pump in stripping nutrients out. One way of demonstrating the role of transport and the biological pump is by comparing our biotic simulation to an abiotic simulation initialized with the same observed nitrate concentration. The abiotic year 3 upper 23-m annual mean nitrate concentrations are well in excess of 5 mmol m^{-3} almost everywhere (Figure 20c). By contrast, the year 3 annual mean of the biotic model has nitrate concentrations of less than 1 mmol m^{-3} over most of the basin (Figure 20b), with removal of ~90% or more of the nitrate that would otherwise accumulate (Figure 20d). In these regions the stripping out of nutrients by the biological pump is highly efficient relative to the supply rate.

On the other hand, biotic removal is less than 90% and surface concentrations are greater than 1 mmol m^{-3} in zones of deep wintertime convection in the subpolar and northern half

Mean (100 W - 24 E), (0 - 23 m)

(a) Potential nitrate limitation term
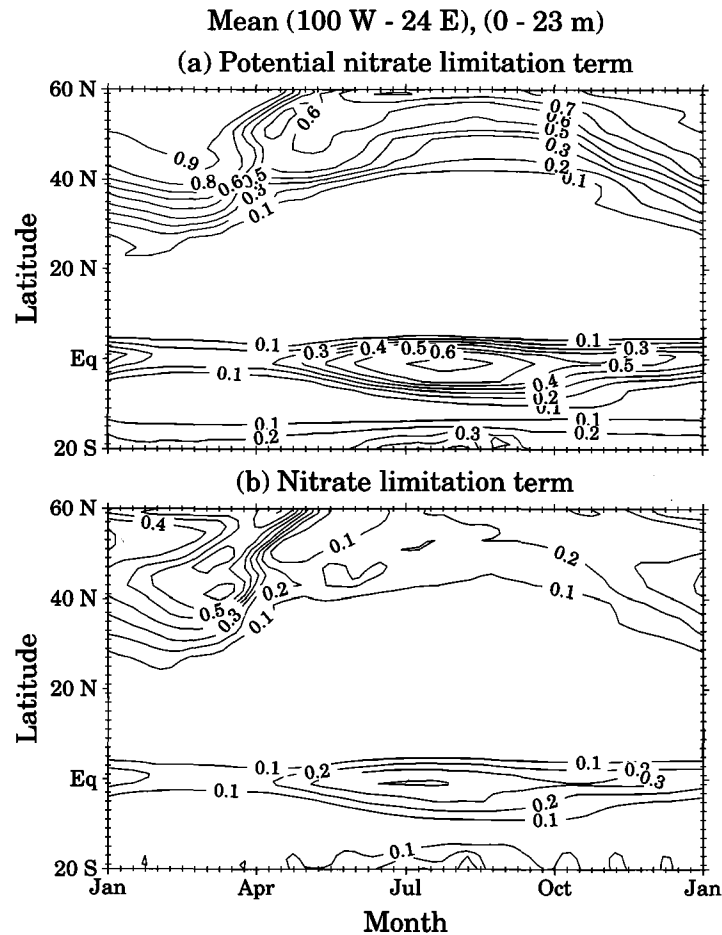

(b) Nitrate limitation term

Fig. 16. Time latitude plots of zonal mean (a) potential nitrate uptake and (b) nitrate uptake in the upper 23 m. The contour interval is 0.1. Nitrate uptake is $Q_1(N_n, N_r)$ defined by (3), and potential nitrate uptake is $Q_1(N_n, N_r)$ divided by $e^{-\psi N_r}$ the ammonium inhibition term .

of the subtropical gyres, as well as the area of strong upwelling in the southwestern corner of the model adjacent to Africa (Figures 20b and 20d). The biological pump strips out a substantial fraction of the nitrate that would accumulate if the ocean were abiotic. However, the input by transport is large enough relative to photosynthetic uptake to give results that differ significantly from those described in the previous paragraph.

The objective of this section is to develop a paradigm for what controls surface nutrient concentrations in terms of the distinction between biologically and transport dominated systems suggested by the above results. The dividing line is difficult to define, particularly since the steady state transport and photosynthetic uptake must balance each other exactly. However, the usefulness of the concept in explaining surface nutrient concentrations is readily portrayed. A system dominated by photosynthetic uptake will have nutrient concentrations of the order of the half-saturation constant for nutrient uptake (0.5 mmol m-3 in our nitrate based model). A system dominated by transport will tend towards nutrient concentrations that approach those of the nutricline (O(10)

mmol m-3 nitrate in our model). The most dramatic contrasts in surface nutrient concentration are those that exist between regions such as the Equatorial Pacific or the North Atlantic, particularly in winter, where nitrate approaches values of order 10 mmol m-3; and the Equatorial Atlantic in winter and the subtropical gyre, where nitrate is of order 1 mmol m-3 or less. These features are all reproduced either in the model described here (Figures 14 and 20), or in simulations that will be described elsewhere.

The high winter nutrient concentrations of the North Atlantic are relatively straightforward to explain. The light supply is inadequate to support photosynthesis. The model thus approximates the abiotic simulation described above, with transport (primarily winter convection) driving nutrients into the surface. Nitrate concentrations increase to levels in excess of 10 mmol m-3 before the return of the sun and onset of stratification enable the phytoplankton to begin stripping nutrients out again (Figure 14) [Yentsch, 1990]. The Equatorial Pacific is never abiotic, but the capacity of the model ecosystem to take up nitrate is inferior to the increase in total (vertical + horizontal) supply rate that would occur if
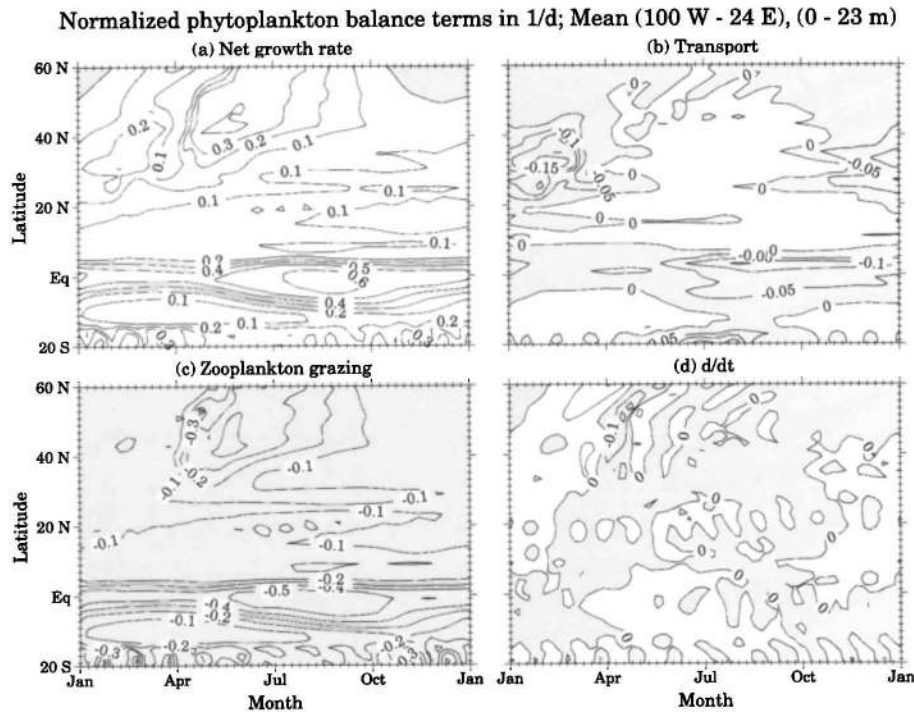
Normalized phytoplankton balance terms in 1/d; Mean (100 W - 24 E), (0 - 23 m)

Fig. 17. Upper 23 m time latitude plot of zonal mean terms in P-normalized phytoplankton balance equation. All terms have units of d[-1]. Normalized (a) net production, (b) transport, (c) zooplankton grazing, and (d) time rate of change of phytoplankton

surface concentrations were lower. The equilibrium surface concentration must be high enough to reduce the supply to a level the phytoplankton can cope with. The limitation of phytoplankton concentration resulting from zooplankton grazing plays an important role in fixing the upper limit of the photosynthetic nitrate uptake rate. One can therefore think of both the Equatorial Pacific and wintertime North Atlantic ecosystems as saturated with nutrients. Nutrient concentrations are determined primarily by the requirement that total nutrient input be kept down to levels the ecosystem can cope with. Other regions of the Atlantic simulation that exhibit this behavior are the southwest near Africa (Figure 20b), where high upwelling occurs due in part to the wall boundary condition, and, to a lesser extent, some areas of the summertime North Atlantic and Equator.

By contrast, the capacity of phytoplankton to take up nutrients in much of the summertime North Atlantic and all of the wintertime Equatorial Atlantic is not saturated. Here nitrate concentrations are kept down to the order of magnitude of the half-saturation constant for photosynthetic uptake, i.e., 0 5 mmol m^{-3} (Figures 14 and 20). If nitrate supply were increased, the nutrient concentration would increase only by the small amount required for phytoplankton to take up nitrate at the same rate it is supplied. One can therefore think of the nutrient concentration in these systems as determined predominantly by photosynthetic uptake.

It is helpful for purposes of this discussion to consider the behavior of a simple box model with a nutrient flux $F(N_n) = v(N_n^* - N_n)$ (where v is exchange velocity with a deep reservoir of fixed nitrate concentration N_n^*) balanced by

photosynthetic uptake $SMS(N_n) = -P\bar{J}N_n/(K + N_n)$. Recall that $\bar{J}$ is the light limited growth rate defined by (4). A steady state solution is obtained from the balance $\partial N_n/\partial t = F(N_n + SMS(N_n)) = 0$ using K=0.5 mmol m^{-3}, $P\bar{J}$ =(0.5 mmol m^{-3})•(1 d^{-1})=0.5 mmol m^{-3} d^{-1}, and N_n^* = 12 mmol m^{-3}, as values representative of the GCM ecosystem model at the Equator (Figure 21a). Results are also given for $P\bar{J}$ =0.25 mmol m^{-3} d^{-1}, in order to show how changes in the phytoplankton and light limited growth rate affect the results (Figure 21b). The plot of nitrate input versus exchange velocity shown in Figure 21c illustrates the difference in behavior between a system dominated by phytoplankton uptake and one dominated by nitrate transport. The curve defined by the box model consists of two almost straight-line segments separated by a sharp transition. At small velocities phytoplankton are able to maintain surface nutrients at low levels (Figures 21a and 21b). Nitrate transport thus increases almost linearly with exchange velocity. At high velocities the phytoplankton uptake capacity becomes saturated. The steady state nitrate input, which is required to balance the uptake, thus becomes fixed at the upper limit of phytoplankton uptake. This condition is satisfied, in the face of increased exchange velocity, by the reduction in vertical nitrate gradient resulting from increased surface nitrate concentration (Figures 21a and 21b).

Physical transport processes in the GCM are too complex to represent by a single number such as the exchange velocity. However, the transition between phytoplankton uptake dominated and transport dominated systems is also illustrated by the relationship between nitrate and nitrate input (Figure

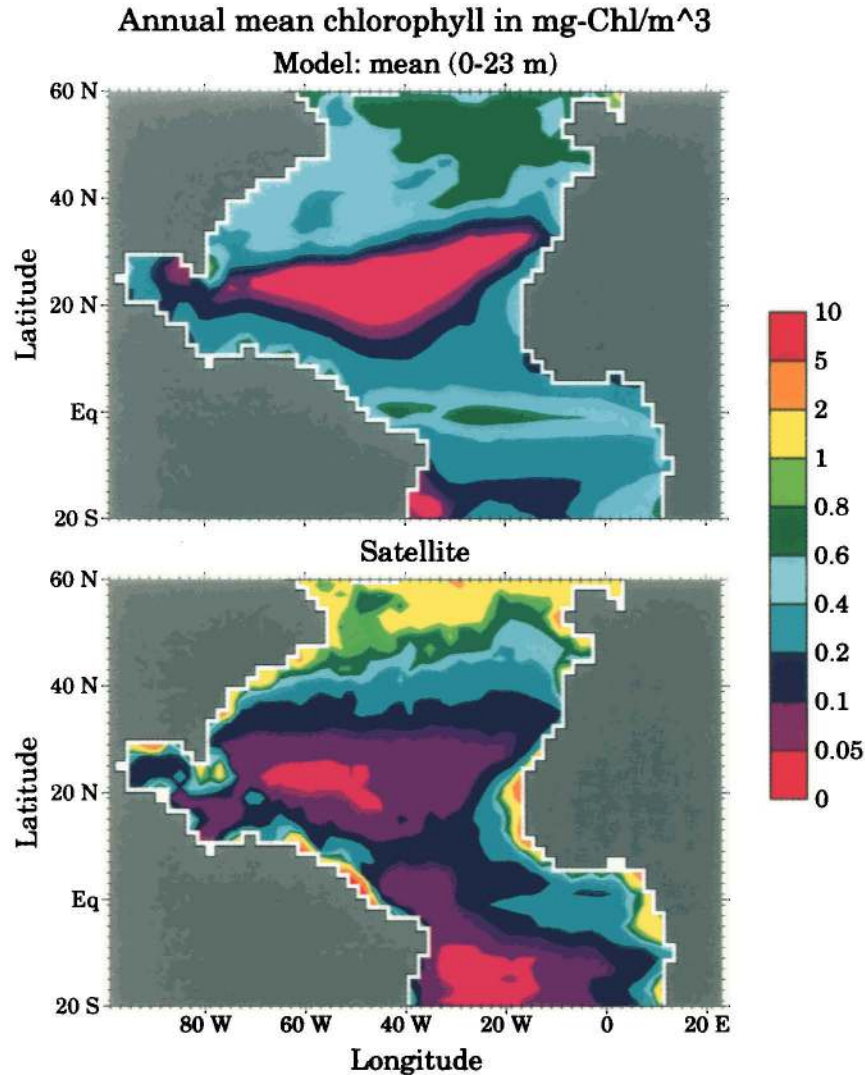## Annual mean chlorophyll in mg-Chl/m^3
Model: mean (0-23 m)

Plate 1. Comparison of (a) annual mean chlorophyll concentrations from the model predicted phytoplankton standing crop for the upper 23 m (two layers) of our model, with (b) the same quantity estimated from satellite CZCS observations [Esaias et al., 1986; Feldman et al., 1989].

22), both of which can be readily obtained from the GCM. The difference in behavior between the equatorial band of the Atlantic and the high latitudes of the North Atlantic in the GCM model is dramatically illustrated by such a plot (Figure 23). The dominant trend of model results in the Figure 24a plot of annual mean nitrate concentration versus annual nitrate supply from the region between 40°N and 60°N is a large increase in nitrate from near 0 to ~8 mmol m^{-3} with a modest increase in nitrate supply from ~7 to ~20 mmol m^{-3} yr^{-1}. By contrast, the equatorial region (5°S to 5°N) exhibits a modest range of 0 to ~2 mmol m^{-3} in mean annual nitrate concentration with a massive increase in annual nitrate supply from 0 to ~68 mmol m^{-3} yr^{-1}. The remainder of the ocean falls mostly within one or the other of these two trends. The high annual mean concentrations of the North Atlantic are a

reflection primarily of the winter (Figures 14 and 23b), when the system is essentially abiotic and thus dominated by transport. Summer nutrients are lower but remain quite high at a number of grid points (Figure 23c). The Equatorial Atlantic, shows an interesting seasonal behavior. During the winter, when transport is at a minimum though still very high (Figure 14), photosynthetic uptake is adequate to keep surface nutrients within the range of the half-saturation constant for nitrate uptake everywhere (Figure 23b). However, the higher nitrate supply of the summertime Equatorial Atlantic (Figure 14), overwhelms the photosynthetic uptake at a number of grid points, leading to a significant increase in nitrate concentration (Figure 23c).

A convenient definition for the boundary between transport dominated and photosynthetic uptake dominated systems in the
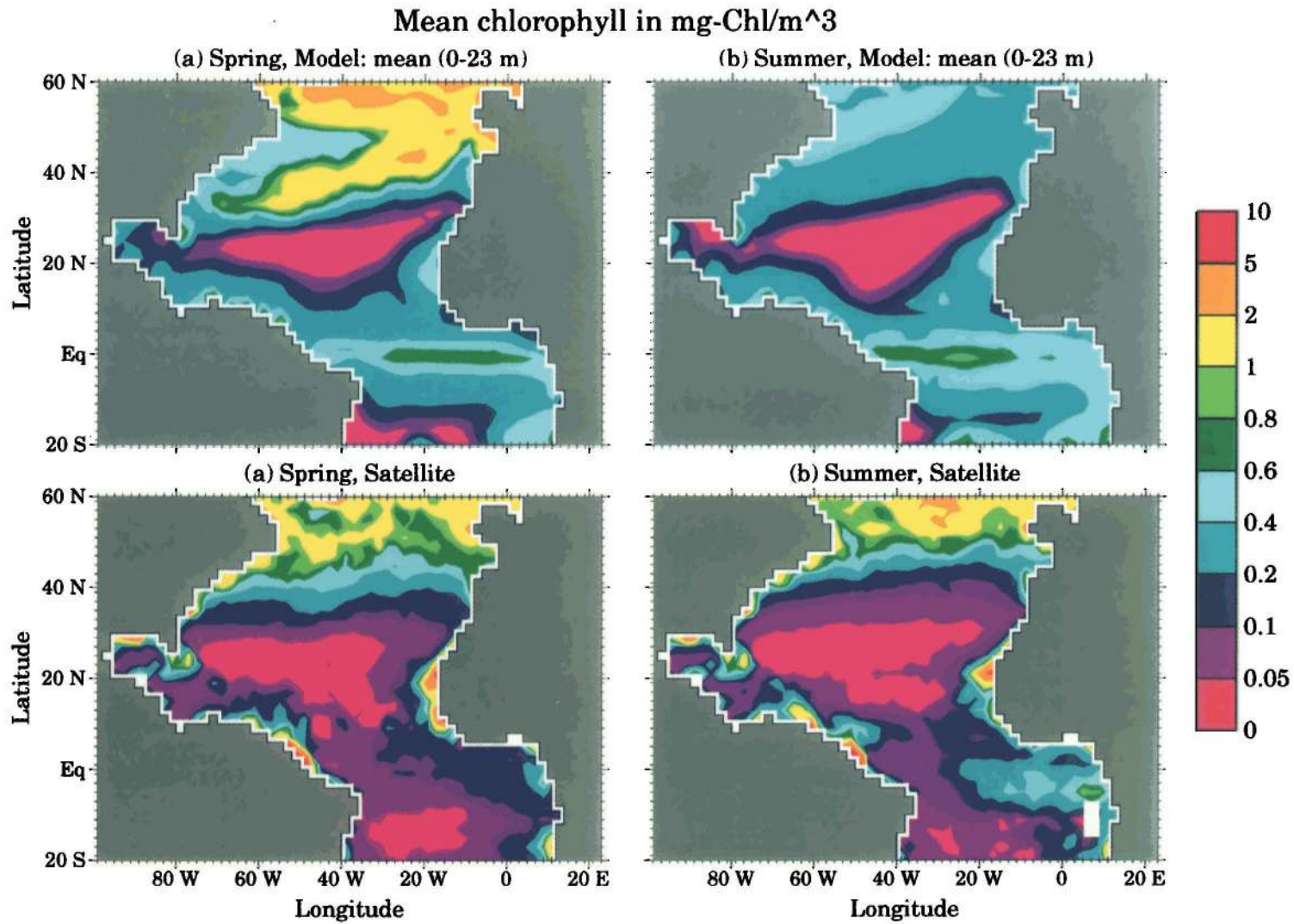
Mean chlorophyll in mg-Chl/m^3

Plate 2. Seasonal chlorophyll averages predicted by the model compared to CZCS observations. Spring is April, May, and June, etc. Yoder et al. [1993] show that the CZCS observations are too high poleward of 40°N during the months of September or October to December.
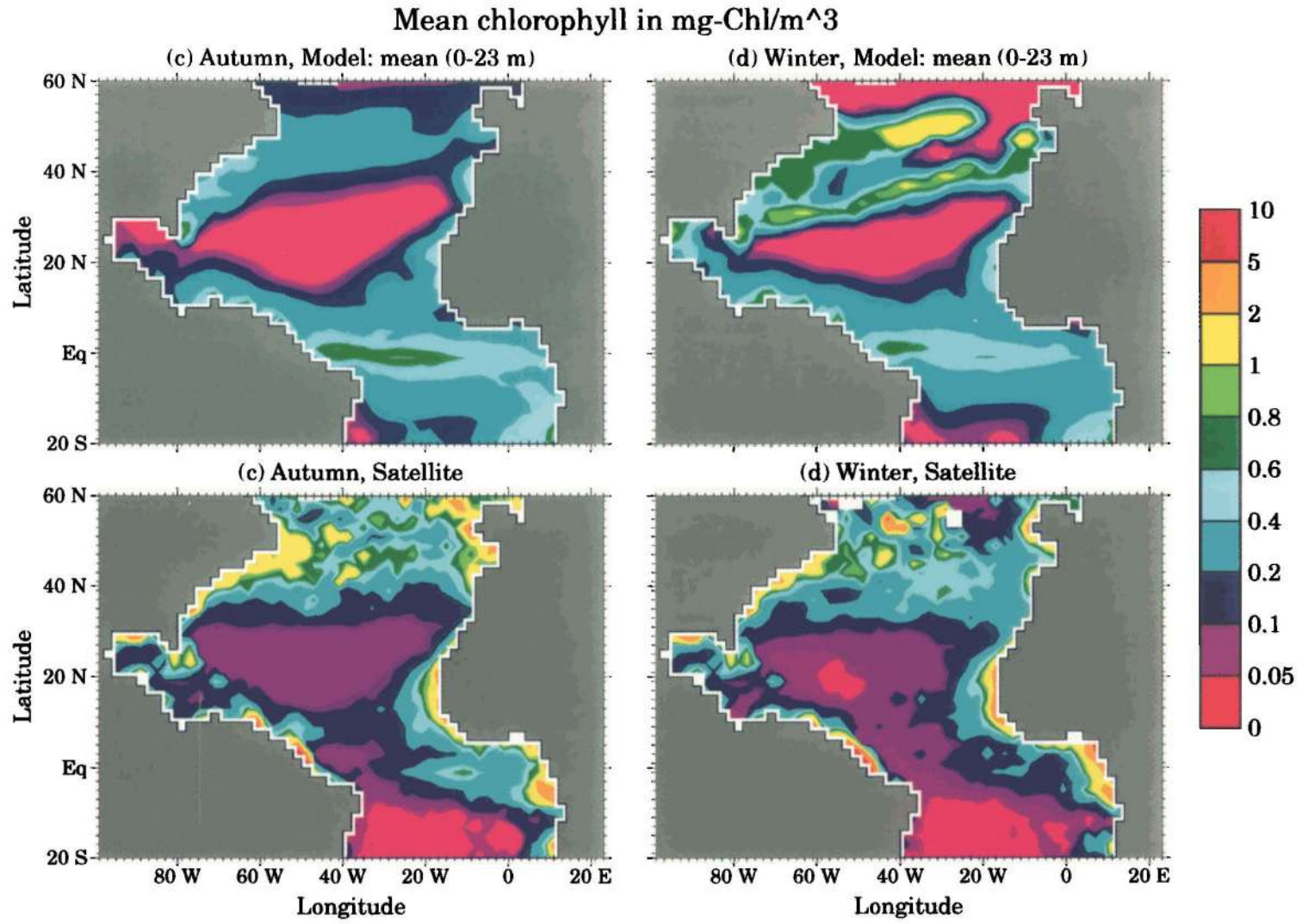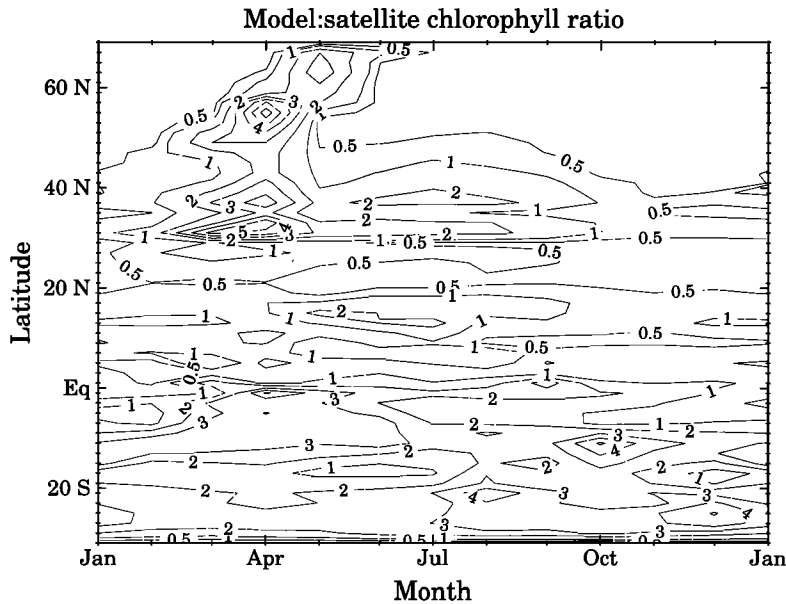
Mean chlorophyll in mg-Chl/m^3

Plate 2.(continued)

Model:satellite chlorophyll ratio

Fig. 18. Zonal mean time latitude plot of the ratio of chlorophyll content estimated from model phytoplankton to chlorophyll estimated from CZCS observations. The contour interval is 0.5, 1, 2,...
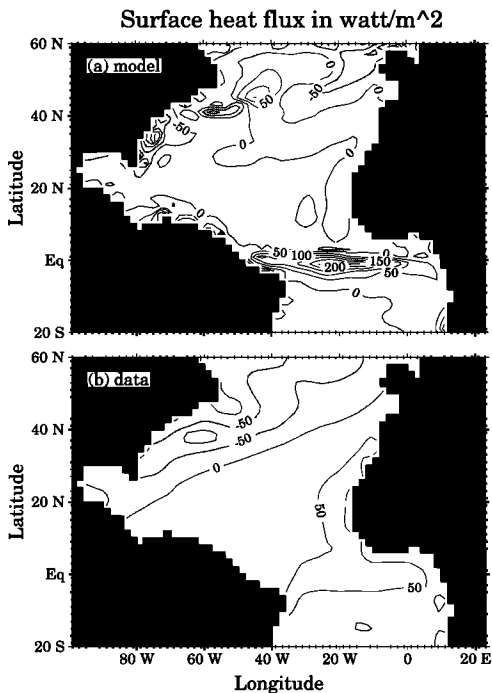
Surface heat flux in watt/m^2

Fig. 19. Surface heat flux in W m^{-2} obtained from the ocean model of Sarmiento [1986]; (upper panel) and from observations as analyzed by Esbensen and Kushnir [1981]; (lower panel). Stippling indicates heat loss from the ocean. Note that the southern half of the subtropical gyre in the model is losing heat, whereas the observations suggest there should be heat gain. Also note that the equatorial heat gain in the model is much more intense than in the observations.

box models is the intersection of a straight-line fit to the nitrate input $F(N_n)$ versus exchange velocity v curve at $v = 0$ (which has a slope equal to the lower layer nitrate concentration, N_n^*) with the maximum potential phytoplankton uptake $SMS(N_n) = P\bar{J}N_n^*/(K + N_n^*)$. This intersection occurs at $v = 0.04$ m d^{-1} when $P\bar{J} = 0.5$ mmol m^{-3} d^{-1}, and at $v = 0.02$ m d^{-1} when $P\bar{J} = 0.25$ mmol m^{-3} d^{-1}.

An alternative approach which gives the same result is to consider how a steady state model responds to a small nitrate perturbation. In steady state in the photic zone, net physical supply of nitrate is balanced by phytoplankton uptake. If nitrate is added, both of these terms will change in a way that ultimately restores the balance. Initially, one term might change more than the other. If the phytoplankton uptake term initially changes more than the net physical transport term, we call the system "uptake restored," which corresponds to our uptake dominated system; otherwise we call the system "transport restored," corresponding to our transport dominated system. The sensitivity of transport and photosynthetic uptake to a perturbation in nitrate concentration in the box model can be found from the derivative

$$\frac{\partial}{\partial N_n}\left(\frac{\partial N_n}{\partial t}\right) = \left(\frac{\partial F(N_n)}{\partial N_n}\right) + \left(\frac{\partial SMS(N_n)}{\partial N_n}\right)$$

$$= (-v) + \left(-P\bar{J}\frac{K}{(K+N_n)^2}\right)$$

The boundary between an uptake restored and transport restored system is found by setting the flux and uptake derivatives equal to each other, i.e., $\partial(\partial N_n/\partial t)/\partial N_n = 0$, and solving the resulting equation for N_n in terms of v. This solution gives the lines shown in Figures 21a and 21b, which define the

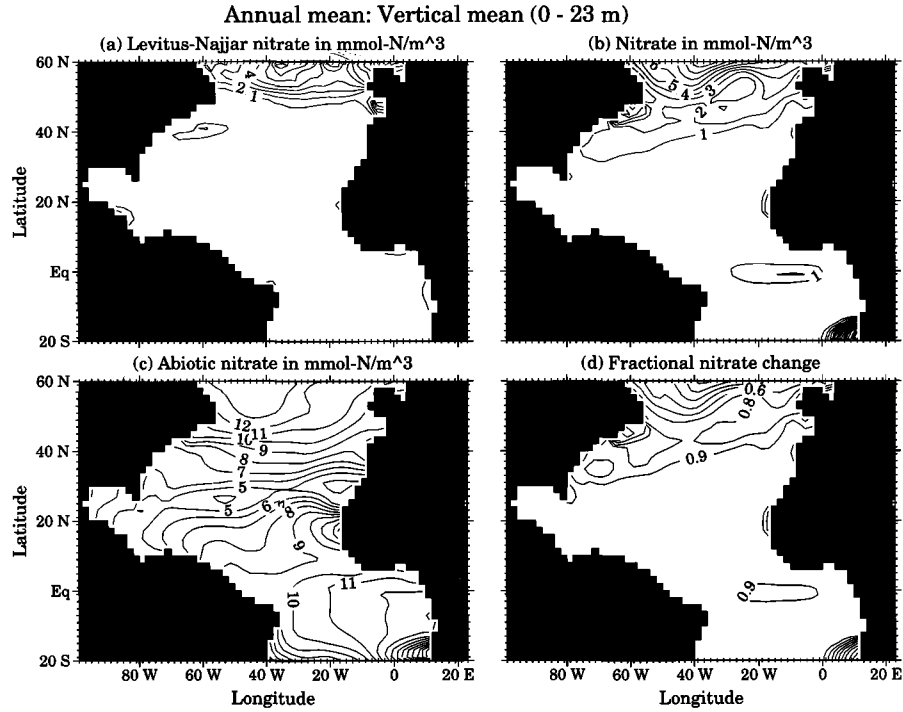## Annual mean: Vertical mean (0 - 23 m)

Fig. 20. (a) Observed annual mean nitrate in the upper 23 m as mapped by S. Levitus and R. Najjar (personal communication, 1992). (b) Annual mean nitrate predicted from the three year biotic simulation. (c) Same as (b) but for the abiotic model. (d) Percent of abiotic nitrate change removed in simulation with biology. Contour interval for nitrate is 2.0 mmol m^{-3}.

boundary between a transport restored ecosystem above, and an uptake restored ecosystem below. The equilibrium nitrate concentration falls within the uptake restored region below an exchange velocity of 0.04 m d^{-1} for $P\bar{J}$=0.5 mmol m^{-3} d^{-1}, and below 0.02 m d^{-1} when $P\bar{J}$=0.25 mmol m^{-3} d^{-1}, in agreement with the approach discussed in the previous paragraph. The equilibrium nitrate content at the uptake restored-transport restored boundary is $K(-1+\sqrt{1+N^*/K})=$ 2 mmol m^{-3}. Note that it is insensitive to $P\bar{J}$.

It is difficult (though possible) in a model of the complexity of our GCM ecosystem model to calculate exactly where the change from uptake restored to transport restored takes place. The box model results (Figures 21a and 21b) and GCM model results at the equator (Figure 21a) suggest as a reasonable approximation that the nitrate concentration at which the model switches from being uptake restored to transport restored is not sensitive to phytoplankton or the light limited growth rate $\bar{J}$ and that it occurs when nitrate concentration increases above the level required to give $N_n/(K+N_n) \sim 0.8$, i.e., when $N_n \sim 2$ mmol m^{-3}. The magnitude of the nitrate input at the transition is sensitive to $P\bar{J}$ (Figure 21c). The lower $P\bar{J}$ of the North Atlantic explains why the transition occurs as lower nitrate inputs than in the Equatorial region (Figure 23).

Having developed the basic concept, we turn now to an examination of the GCM nitrate balance equation,

$0 = T(N_n) + SMS(N_n)$, with $SMS(N_n)$ defined by (2), (3) and (4), from which one can obtain

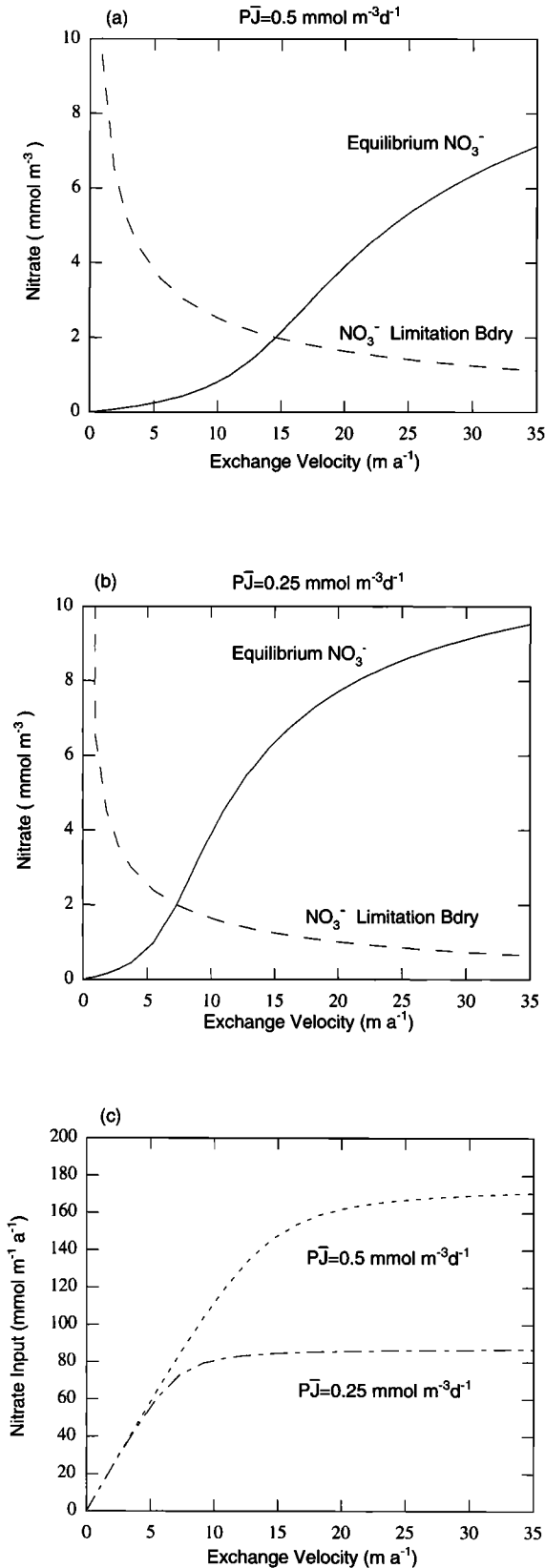$$N_n = K_1 \frac{\beta}{1-\beta} \qquad (8)$$

with

$$\beta = \frac{T(N_n)}{P\bar{J}(z,t)e^{-\psi N_r}}$$

The box model analysis would suggest a high correlation between transport and β in uptake restored systems, as is in fact observed in Figure 24a. β is also positively correlated with the inverse of the ammonium inhibition term, $1/e^{-\psi N_r}$ (Figure 24b), but the fractional increase in this term is far too small to explain the increase in β. Furthermore, the inverse of the phytoplankton concentration, $1/P$ is negatively correlated with β (Figure 24d), and its trend almost exactly cancels the trend in $1/e^{-\psi N_r}$ such that the combined contribution of these two terms, $1/Pe^{-\psi N_r}$ to the trend in β is negligible. On the other hand, the large scatter in $T(N_n)$ for a given β can be accounted for primarily by the contribution from the large scatter in $1/P$. The light limited growth term, $1/\bar{J}(z,t)$, is essentially constant. In the equatorial region, the maximum annual mean value of β is 0.8, which gives the upper limit of 2 mmol m^{-3} for annual mean nitrate shown in Figure 23a.

The high annual mean nitrate concentrations of the high latitude North Atlantic are mainly due to the low wintertime

(a) $P\bar{J}=0.5$ mmol m^{-3}d^{-1}

Equilibrium NO$_3^-$

NO$_3^-$ Limitation Bdry

Nitrate (mmol m^{-3})

Exchange Velocity (m a^{-1})

(b) $P\bar{J}=0.25$ mmol m^{-3}d^{-1}

Equilibrium NO$_3^-$

NO$_3^-$ Limitation Bdry

Nitrate (mmol m^{-3})

Exchange Velocity (m a^{-1})

(c)

$P\bar{J}=0.5$ mmol m^{-3}d^{-1}

$P\bar{J}=0.25$ mmol m^{-3}d^{-1}

Nitrate Input (mmol m^{-1} a^{-1})

Exchange Velocity (m a^{-1})

supply of light already discussed above. Figure 24 shows that the transport is relatively small, as is the inverse of the phytoplankton concentration (i.e., phytoplankton concentration is relatively high, at least in the annual mean). The high values for the parameter β result primarily from low-light supply giving a large value to $1/\bar{J}$, and also from a small ammonium inhibition term (i.e., a strong inhibition of nitrate uptake by high ammonium concentrations), which shows up as a large $1/e^{-\psi N_r}$ in Figure 24b.

An important part of the overall story is what limits the phytoplankton concentration. For example, the Equatorial Atlantic phytoplankton concentration changes by only approximately a factor of 2 over the large range in nutrient supply (Figure 25a). As indicated above, phytoplankton concentration is limited primarily by zooplankton grazing. Thus, to a first approximation, P is equal to that value which gives a zooplankton growth rate equal to its mortality [Evans and Parslow, 1985]. A more quantitative analysis is obtained by solving the zooplankton balance equation for phytoplankton. Combining (1) and (2) for Z with (5), and rearranging gives P concentration as a function of B, the bacterial concentration; N_p, the particulate organic nitrogen concentration; and $T(Z)/Z$, the normalized transport and time rate of change of zooplankton term.

$$P = \frac{\alpha}{2} + \left[\left(\frac{\alpha}{2}\right)^2 + \rho_2\left(\frac{\alpha}{\rho_1}B - B^2\right) + \rho_3\left(\frac{\alpha}{\rho_1}N_p - N_p^2\right)\right]^{1/2} \quad (9)$$

with

$$\alpha = \frac{[(\mu_2 + \mu_5) - T(Z)/Z]}{\gamma_2 g/K_3 - [(\mu_2 + \mu_5) - T(Z)/Z]}$$

All the terms in α are constants except for $T(Z)/Z$, If we assume $T(Z)/Z$, = 0, the value of α obtained from the parameter values given in Table 2 is 0.125 mmol m^{-3}. In such a case, the maximum value P can have, obtained when B and N_p are 0.25 mmol m^{-3}, is 0.342 mmol m^{-3}. Notice that the amount of P required to produce a certain amount of grazing is higher when bacteria and and particulate organic nitrogen are present. This is a consequence of the choice of switching algorithm. This issue is discussed further by M. J. R. Fasham and G. T. Evans (personal communication, 1992). The reason P can take on values above 0.342 mmol m^{-3}, as illustrated in Figures 10a and 25a, is because of the contribution from $T(Z)/Z$,, the normalized zooplankton

Fig. 21. Results from a steady state box model balance between transport and photosynthesis. Plots of nitrate versus exchange velocity for (a) a model with $P\bar{J} = 0.5$ mol m^{-3} d^{-1} and (b) a model with $P\bar{J} = 0.25$ mol m^{-3} d^{-1}. The solid line is the equilibrium nitrate calculated from the model. The dashed line marks the boundary between an uptake dominant/restored system below the line, and a transport dominant/restored system above the line. (c) Nitrate transport versus exchange velocity for the models with $P\bar{J} = 0.5$ mol m^{-3} day^{-1} and $P\bar{J} = 0.25$ mol m^{-3} day^{-1}.
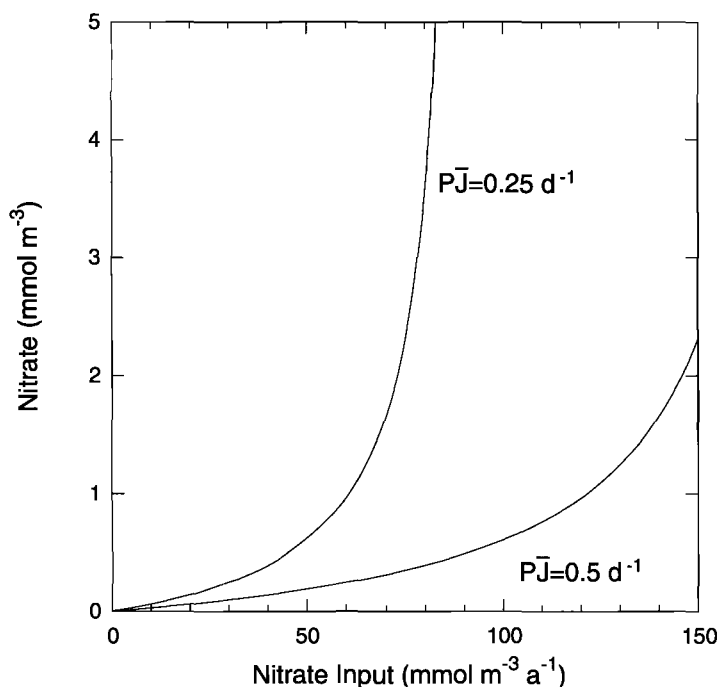
Fig. 22. Nitrate versus nitrate input for the box model.

transport and time rate of change term. The increasing trend with increasing nitrate transport is due in part to increases in B and N_p, and in part to an increase in the rate at which Z is transported away from the area. Removal of Z by transport results in part from the fact that large nutrient supply rates occur in regions of high upwelling that are associated with strong horizontal divergence. Also contributing is the fact that Z concentration becomes larger with increased nitrate input (Figure 25b).

In conclusion, we have found that a useful paradigm for understanding the uptake of nitrate in the model is the definition of uptake restored or dominant and transport restored or dominant suggested above, coupled together with the observation that zooplankton is usually present in high enough concentrations to prevent phytoplankton from expanding beyond a point determined primarily by a balance between zooplankton grazing and mortality. We find that most of the model is uptake dominated/restored, i.e., additional nitrate supplied to the model would go primarily into photosynthesis. There are several regions of the model that are transport dominated/restored, i.e., where additional nitrate supplied by the model would go primarily into increasing the ambient nutrient concentration so as to maintain the transport at a constant value. These are the high latitudes during the winter time and the southwestern corner of the model near Africa, which is affected by high upwelling in the wall region. Finally, there is the phenomenon of the spring bloom, during which zooplankton respond belatedly to phytoplankton such that the phytoplankton can go to very high concentrations. What this does, in terms of our paradigm, is to increase the capacity of the ecosystem to take up nitrate (cf. Figure 21).

This model has a limited capacity to take up nutrients which results from grazing control of phytoplankton population. This, in turn, leads to regions of the model where nutrients remain high. If future investigations show that the maximum phytoplankton levels are controlled by iron limitation, this implies that the effect of grazing in this model has been exaggerated.

4.3. Relationship Between New and Primary Production

Perhaps the only measurement technique that offers the promise of giving high temporal and spatial resolution of any aspect of the biological pump is satellite color observations of the upper ~10 m of the water column. Techniques have been or are being developed for estimating surface chlorophyll concentration from these measurements [Clark, 1981], and for estimating the vertically integrated chlorophyll content from the surface concentration [Platt et al., 1992]. There are well-developed approaches for estimating primary production from vertical profiles of chlorophyll and the light supply [Platt and Gallegos, 1980], and a variety of algorithms for estimating primary production directly from the satellite ocean color observations [Balch et al., 1992]. A major obstacle in making use of satellite color observations for studying the impact of the biological pump on ocean chemistry is how to translate estimates of primary production obtained by these approaches into information on the surface concentration of chemicals resulting from the flux of organic matter out of the surface ocean. Dugdale et al. [1989] used satellite observations of sea surface temperature to estimate surface nitrate levels, and an uptake model to predict new production, which is presumed to
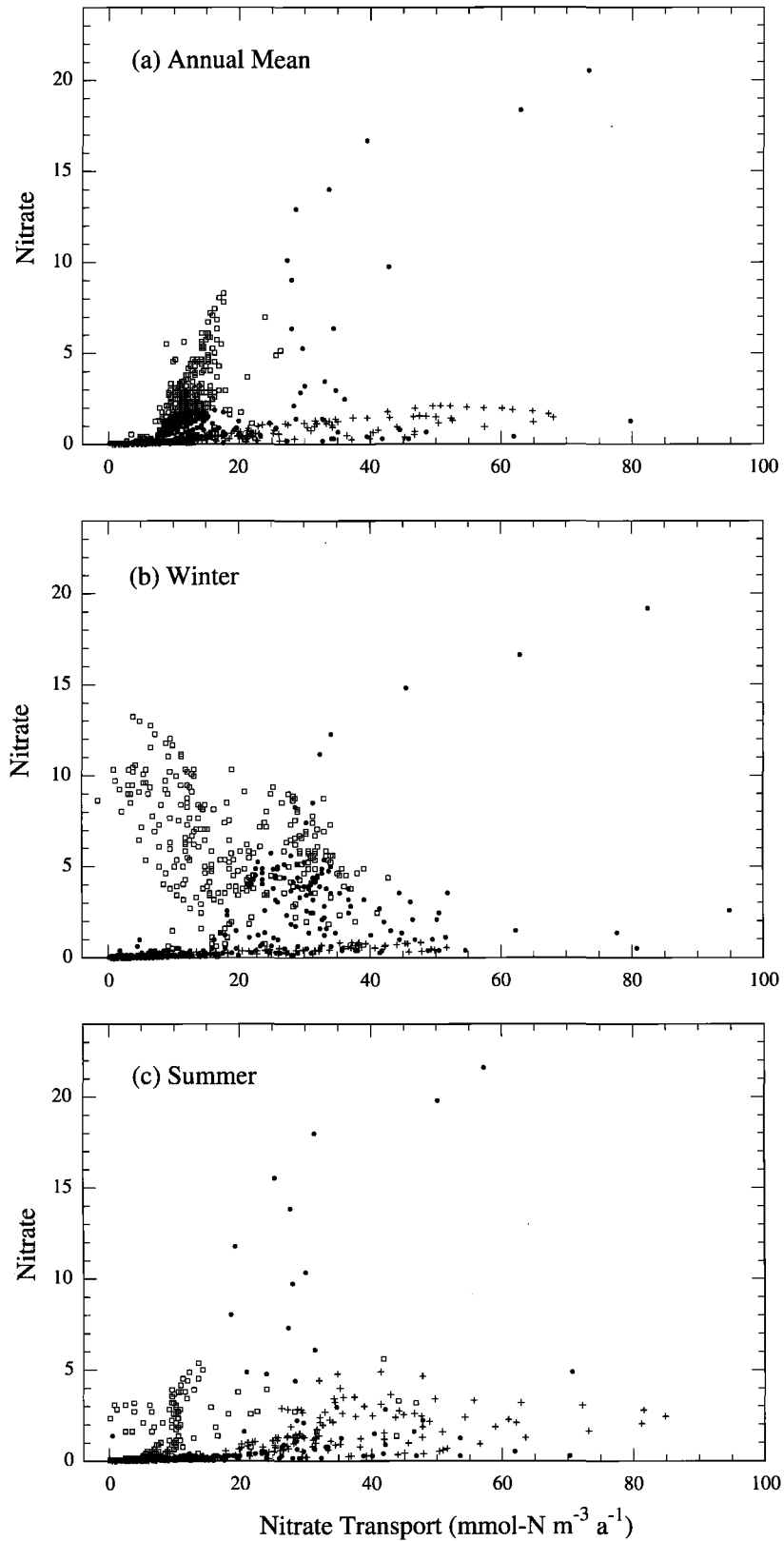
Fig. 23. Plots of the upper 23 m (a) annual mean, (b) winter, and (c) summer mean nitrate concentration in mmol m^{-3} versus mean nitrate transport in mmol m^{-3} yr^{-1} for each grid in the model. Open squares are for grid points between 40°N and 60°N, plus symbols are for the Equator between 5°N and 5°S, and dots are for results from the remainder of the model.
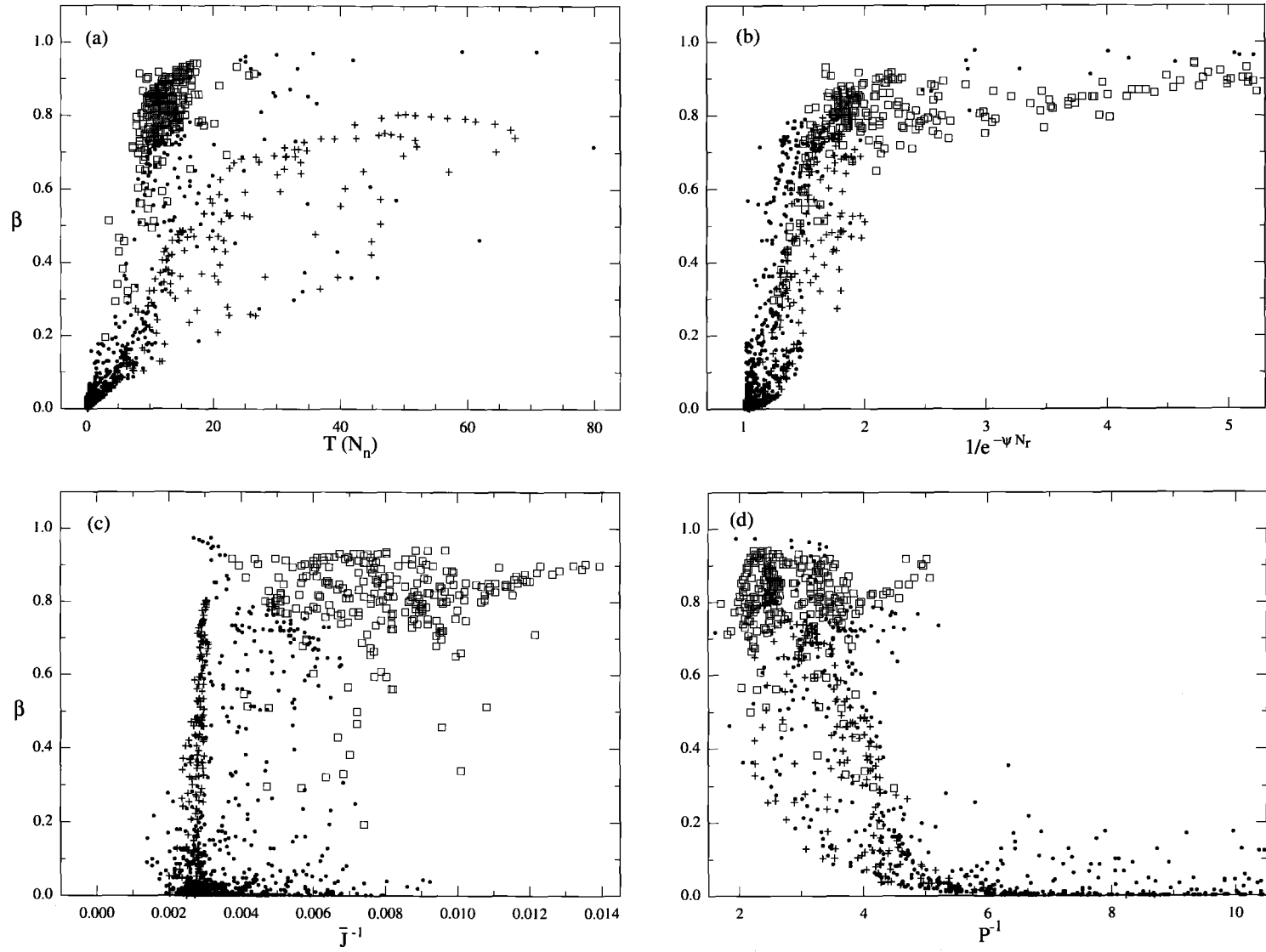
Fig. 24. Plots of the upper 23 m annual mean of ß defined by (8), versus the annual mean of each of the terms in ß: (a) transport $T(N_n)$, (b) the inverse of the ammonium inhibition term $e^{-\psi N_r}$, (c) the inverse of the light limited maximum growth rate $\bar{J}$, and (d) the inverse of phytoplankton P.
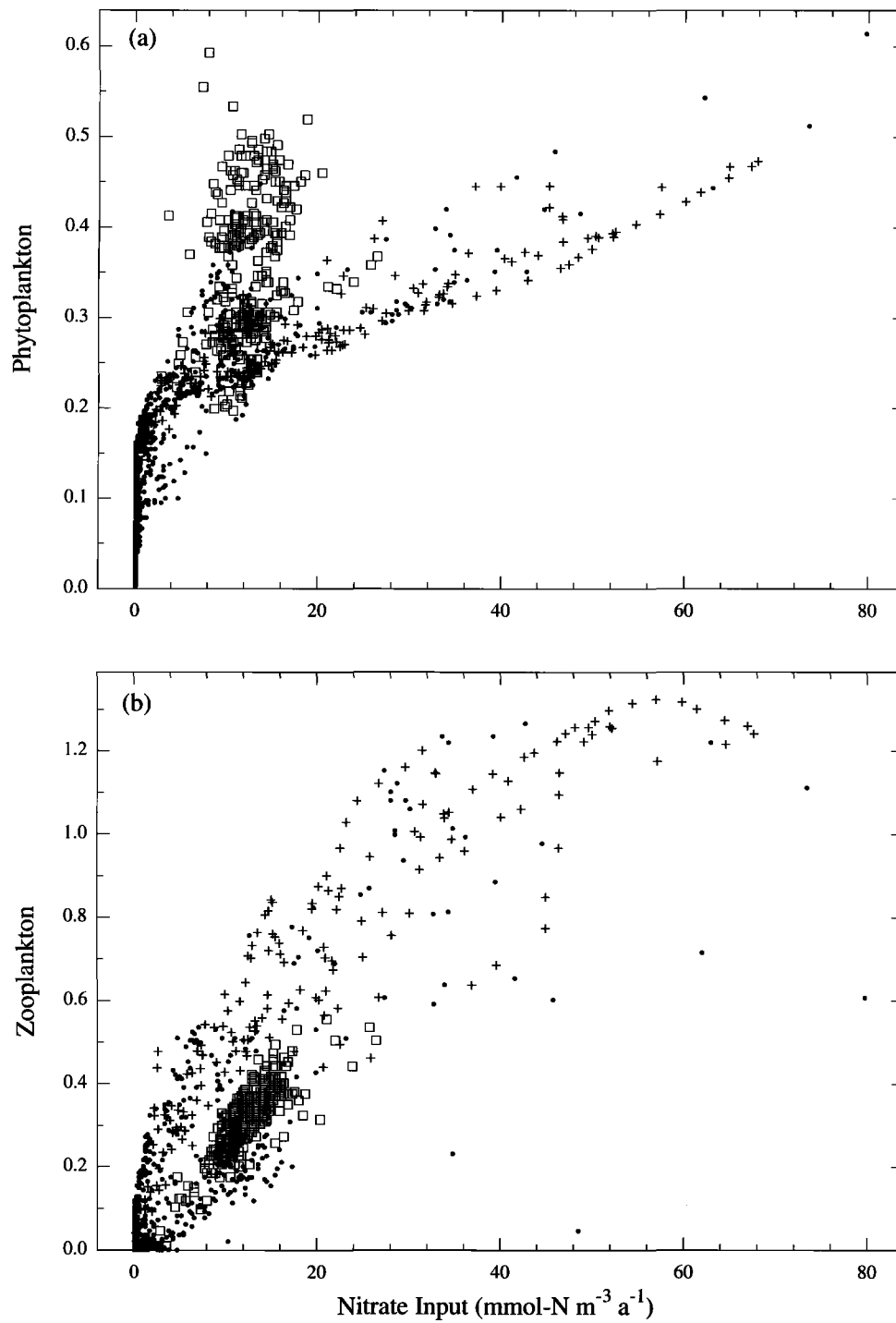
Fig. 25. Plots of the upper 23 m annual mean (a) phytoplankton and (b) zooplankton concentration in mmol m^{-3} versus annual mean nitrate transport in mmol m^{-3} yr^{-1} for each grid in the model. Open squares are for grid points between 40°N and 60°N, plus symbols are for the Equator between 5°N and 5°S, and dots are for results from the remainder of the model.
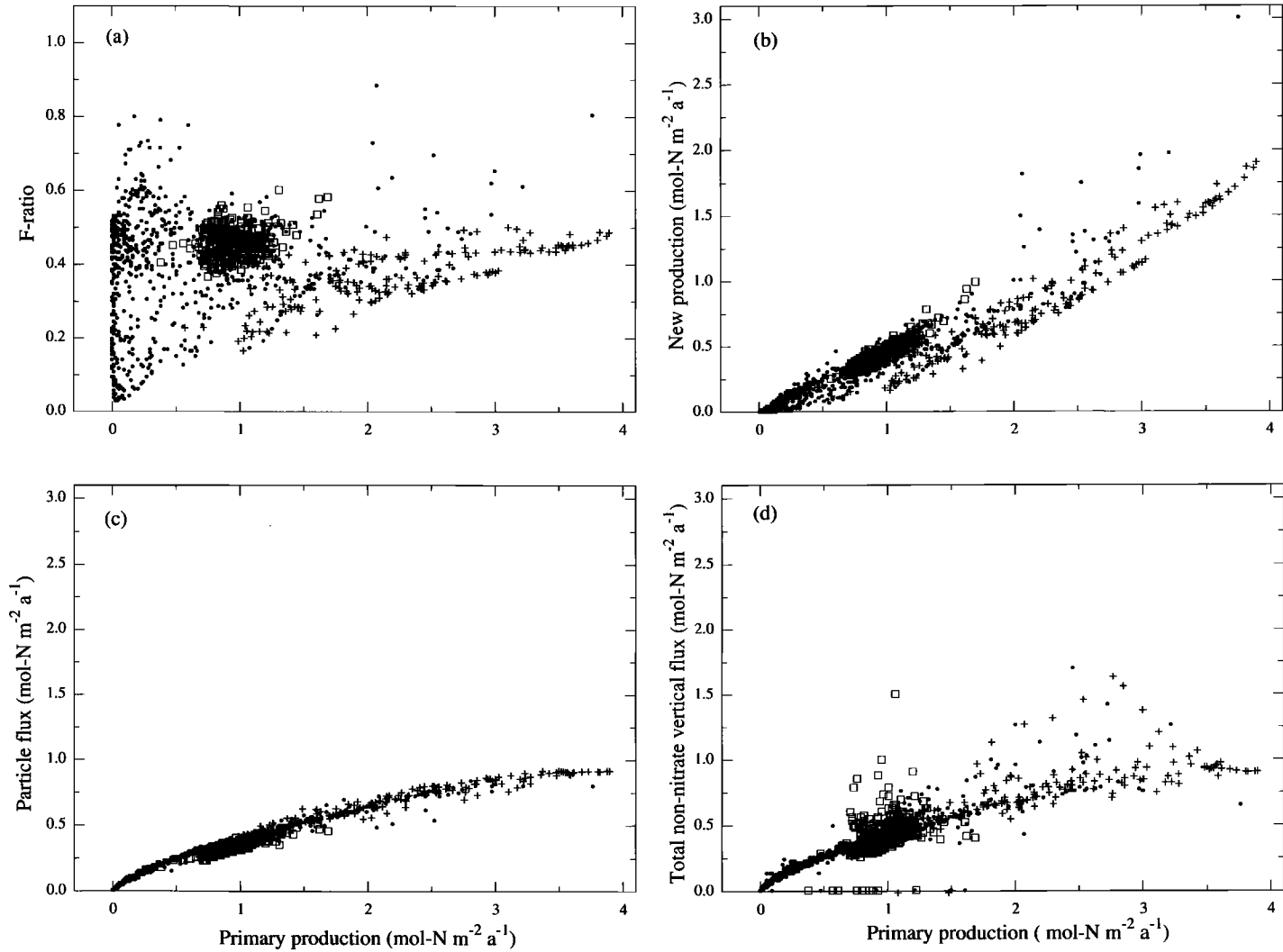
Fig. 26. Relationship between the upper 123 m annual mean of various model predicted properties and the annual mean of the primary production. (a) f ratio, (b) new production, (c) particle flux, and (d) total vertical flux including non-detrital transport of all model compartments except nitrate. The total vertical flux is 0 for grid points that have the ocean floor shallower than 123 m.

equal the export production, from the estimates of nitrate and CZCS chlorophyll. However, it is doubtful that one can count on a correlation between temperature and nitrate to be useful throughout most areas of the ocean. Inasmuch as the organic matter flux must ultimately equal the new production, the quantity that needs to be known is the f ratio. One approach that is being attempted is to establish a relationship between the f ratio and quantities such as primary production or nitrate [Eppley and Peterson, 1979; Eppley, 1989; Harrison et al., 1987]. One purpose of this section is to comment on the insights the model offers as to these relationships. The other purpose is to show how the new and regenerated production are affected by changes in the ecosystem model per se. One of the interesting results from this model is that the new production is relatively insensitive to changes in the ecosystem structure and parameters, whereas the regenerated production varies over a large range.

Figure 26a shows the annual mean f ratio plotted versus annual mean primary production for the upper 123 m of every grid point in our model. These results do not support the simple relationship Eppley and Peterson [1979] propose based on their limited data set. However, the large degree of scatter may be misleading. A plot of new production, i.e. photosynthetic nitrate uptake, versus primary production shows that most of the new production numbers fall within an envelope of ~0.4 mmol m⁻² yr⁻¹ of nitrogen, with the envelope actually becoming smaller at small primary production numbers (Figure 26b),[cf. Eppley and Peterson, 1979]. The f ratio scatter is larger at low primary productions mainly because the denominator is smaller. This figure suggests that the relationship between new production and primary production is reasonably well behaved. However, FDM(1990) show that the temporal variation at a given location can be very large (cf. also Figure 12). Thus we believe that the best strategy for analyzing satellite obervations may turn out to be assimilating them into a model such as ours.

It is of interest to note that the particle flux shows a very good correlation with the primary production (Figure 26c), whereas the total nonnitrate vertical nitrogen flux, which includes downward transport of nondetrital components of the ecosystem, shows a worse correlation (Figure 26d). Apparently the physical processes which remove nondetrital components are poorly correlated with the primary production. This would certainly be expected in the high latitudes, where convective overturning occurs in the winter when primary production is at a minimum.

Table 3 shows a summary of annual mean properties of simulations that were carried out with different detrital sinking velocities and phytoplankton mortalities. The new production varies only between 2 and 2.8 mol m⁻² yr⁻¹ of carbon as calculated using C:N=6.625, smaller than the tracer based average of 3 to 4 mol m⁻² yr⁻¹ given by Jenkins and Wallace [1992] for the North Atlantic subtropical gyre. The average model new production is equivalent to 8 to 12 GtC/yr on a global scale, comparable to the new production estimated by Najjar et al.'s [1992] global model, but larger than the Eppley [1989] estimates and smaller than the Packard et al. [1988] estimates mentioned in the introduction. The relatively small variation in the new production, despite large changes in the ecosystem model structure, is a result of the fact that most of

TABLE 3. Sensitivity Studies

Detrital Sinking Velocity, m d⁻¹	Phytoplankton Mortality, d⁻¹	Nitrate, mmol m⁻³	Ammonium, mmol m⁻³	Chlorophyll, mg-Chl m⁻³	New Production, mol-C m⁻² yr⁻¹	Regenerated Production, mol-C m⁻² yr⁻¹	Primary Production, mol-C m⁻² yr⁻¹	f Ratio
1	0.08	5.2	1.1	0.17	2.0	7.2	9.2	0.22
10	0.04	4.3	0.46	0.21	2.6	3.6	6.2	0.43
100	0.035	3.9	0.21	0.20	2.8	2.5	5.3	0.53

Annual mean results for 20°S to 68°N.

the model is uptake controlled so that the nitrate concentration does not vary by much. Thus the upward supply of nitrate is determined primarily by physical processes, which do not change from one simulation to another. The mean regenerated production, on the other hand, varies between a low of 2.5 mol m^{-2} yr^{-1}, and a high of 7.2 mol m^{-2} yr^{-1} in association with an even larger range in mean ammonium concentration. The lowest regenerated production is for the model with a 100 m d^{-1} sinking rate. This high sinking rate removes organic matter from the surface so efficiently that there is very little ammonium formation. Note that chlorophyll, which is calculated directly from phytoplankton, is almost constant. This would be expected in view of the fact that phytoplankton concentration is determined primarily by the balance between the zooplankton grazing and mortality parameters, which are the same in all simulations.

5. CONCLUSIONS

The most important conclusion of this study is that it confirms the feasibility of merging a single generic ecosystem model of a reasonably high level of sophistication with an ocean general circulation model, and obtaining results that are capable of reflecting the large range of biogeochemical behavior of the surface ocean. The technical problems that were encountered were overcome with only modest difficulty, and the model predictions that were obtained compare favorably with satellite color observations (this paper), and with more detailed observations at Bermuda and Ocean Weathership Station India [Fasham et al., this issue].

The model has been used to examine what determines the nitrate concentration in the surface ocean. The only major area of the model where surface nitrate is below 0.1 mmol m^{-3} throughout most of the year is between 4°N and 23°N. Most of the rest of the model has nitrate between 0.1 and <2 mmol m^{-3} throughout the year or during a substantial portion of the year. The concentration of nitrate in these regions is determined by the requirement that it be large enough that phytoplankton can take up nitrate at the same rate at which the physical processes supply it to the surface. We refer to these regions as "uptake restored" because any perturbation to the nitrate content would be compensated primarily by an increase in photosynthetic uptake. The model parameters that determine the nitrate content for a given nitrate supply rate and phytoplankton concentration are the phytoplankton half-saturation constant, light-limited growth rate, and ammonium inhibition parameter (equation (8)). The phytoplankton concentration, in turn, is determined by the zooplankton grazing (equation (9)). The biological model would benefit greatly from improved observational evidence as to the nature of the functional relationships and magnitudes of the model parameters involved in these processes. For example, some of the zooplankton mortality functions examined by Steele and Henderson [1992] could lead to significantly different results.

It was suggested that some areas of the equatorial region have nitrate supply rates to the surface that are close to the limit of the uptake capacity of the phytoplankton (in a steady state the uptake must balance the supply rate). When the phytoplankton become "nitrate replete," that is, when the concentration of nitrate climbs to the point where additional increases are compensated primarily by a reduction in nitrate

transport rather than an increase in photosynthetic uptake, one would expect the surface nitrate concentration to increase. Indeed, this limit is exceeded near the southern wall where there is high upwelling associated with the wall boundary condition, in the high latitudes during the winter, and in some coastal upwelling regions. It is also exceeded in a simulation of the Pacific Ocean equatorial region that will be reported on elsewhere. When this occurs, nitrate concentration climbs well above levels comparable to the phytoplankton half saturation constant of 0.5 mmol m^{-3}, to the point where it is sufficiently large relative to the nitrate content in the waters supplying the surface that the net nitrate transport is reduced to a level the phytoplankton can cope with. An important part of this argument is the requirement that in regions of adequate light and nitrate supply throughout the year, there is an upper limit to phytoplankton concentration imposed by zooplankton grazing [Walsh, 1976; Miller et al., 1991].

The ultimate goal of our project is to use models such as these to develop a greater understanding of the role of the biological pump in the cycles of climatically important chemicals such as carbon dioxide, dimethyl sulphide, and nitrous oxide. We are interested in examining the feasibility of developing prognostic ecosystem models that can be placed in the coupled atmosphere-ocean GCMs that are being used to predict the effect of greenhouse gas increase in climate. We are also interested in the development of tools that can be used to translate satellite measurements of ocean color and other measurements relevant to ocean chemical cycles into information that is useful in monitoring the long-term trends in the effect of the biological pump on ocean chemistry. The first results from this simulation are encouraging, although there are many problems that need to be addressed. This paper has focussed primarily on problems with the ocean physics since these are the ones that stand out in the large-scale analysis that we have carried out. Fasham et al.'s [this issue] more detailed analysis and comparison with biological data also shows problems with the biological model.

REFERENCES

Bacastow, R. B. and E. Maier-Reimer, Ocean-circulation model of the carbon cycle, *Clim. Dyn. 4*, 95-125, 1990.
Bacastow, R. and E. Maier-Reimer, Dissolved organic carbon in modeling oceanic new production, *Global Biogeochem. Cycles, 5*, 71-85, 1991.
Balch, W., R. Evans, J. Brown, G. Feldman, C. McClain and W. Esaias, The remote sensing of ocean primary productivity: Use of a new data compilation to test satellite algorithms, *J. Geophys. Res., 97*, 2279-2293, 1992.

Banse, K., Does iron really limit phytoplankton production in
the offshore Subarctic Pacific?, *Limnol. Oceanogr., 35,*
772-775, 1990.

Benner, R., J. D. Palulski, M. McCarthy, J. I. Hedges and P.
G. Hatcher, Bulk chemical characteristics of dissolved
organic matter in the ocean, *Science, 255,* 1561-1564,
1992.

Bryan, K., A numerical method for the study of the circulation
of the world ocean, *J. Comput. Phys., 4,* 347-376, 1969.

Carpenter, E. J. and D. G. Capone, Nitrogen and the Marine
Environment., 900 pp., Academic, San Diego, Calif.,
1983.

Chisholm, S. W. and F. M. M. Morel, What controls
phytoplankton production in nutrient-rich areas of the open
sea?, *Limnol. Oceanogr., 36,* 1507-1965, 1991.

Clark, D. K., Phytoplankton pigment algorithms of the
Nimbus-7 CZCS, in *Oceanography From Space,* edited by
J. F. R. Gower, 227-237, Plenum, New York, 1981.

Dugdale, R. C. and J. J. Goering, Uptake of new and
regenerated forms of nitrogen in primary productivity,
Limnol. Oceanogr., 12, 196-206, 1967.

Dugdale, R. C., A. Morel, A. Bricaud and F. P. Wilkerson,
Modeling new production in upwelling centers: a case
study of modeling new production from remote sensed
temperature and color., *J. Geophys. Res., 94,* 18119-
18132, 1989.

Eppley, R. W., Temperature and phytoplankton growth in the
sea, *Fish. Bull., 70,* 1063-1085, 1972.

Eppley, R. W., New Production: History, methods, problems,
in *Productivity of the Ocean: Present and Past,* edited by
V. S. Smetacek, G. Wefer and W.H. Berger, pp. 85-97,
John Wiley, 1989.

Eppley, R. W. and B. J. Peterson, Particulate organic matter
flux and planktonic new production in the deep ocean,
Nature, 282, 677-680, 1979.

Esaias, W., G. C. Feldman, C. R. McClain and J. A. Elrod,
Monthly satellite-derived phytoplankton pigment
disribution for the North Atlantic Ocean Basin, *Eos Trans.
AGU, 67,* 835-837, 1986.

Esbensen, S. K. and Y. Kushnir, The heat budget of the global
ocean: An atlas based on estimates from surface marine
observations, *Rep. 29,* Clim. Res. Inst., Oreg. State Univ.,
Corvallis, 1981.

Evans, G. T. and J. S. Parslow, A model of annual plankton
cycles, *Biol. Oceanogr. 3,* 327-347, 1985.

Fasham, M. J. R., Modelling the marine biota, in *The Global
Carbon Cycle,* edited by M. Heimann, Springer-Verlag,
New York, 1992.

Fasham, M. J. R., H. W. Ducklow and S. M. McKelvie, A
nitrogen-based model of plankton dynamics in the oceanic
mixed layer, *J. Mar. Res., 48,* 591-639, 1990.

Fasham, M. J. R., J. L. Sarmiento, R. D. Slater, H. W.
Ducklow and R. Williams, A seasonal three-dimensional
ecosystem model of nitrogen cycling in the North Atlantic
euphotic zone: A comparison of the model results with
observation from Bermuda Station "S" and OWS "India",
Global Biogeochem. Cycles, this issue, 1993.

Feldman, G., N. Kuring, C. Ng, W. Esaias, C. McClain, J.
Elrod, N. Maynard, D. Endres, R. Evans, J. Brown, S.
Walsh, M. Carle and G. Podesta, Ocean color, availability

of the global data set, *EOS Trans. AGU, 70,* 633-648,
1989.

Gordon, H. R., D. K. Clark, J. W. Brown, O. B. Brown and
R. H. Evans, Satellite measurements of the phytoplankton
pigment concentration in the surface waters of a warm core
Gulf Stream ring, *J. Mar. Res., 40,* 491-502, 1982.

Harrison, D. E., On climatological monthly mean wind stress
and wind stress curl fields over the world ocean, *Journal of
Climate, 2,* 57-79, 1989.

Harrison, W. G., T. Platt and M. R. Lewis, f-ratio and its
relationship to ambient nitrate concentration in coastal
waters, *J. Plankton Res., 9,* 235-248, 1987.

Hastenrath, S., Hemispheric asymmetry of oceanic heat budget
in the equatorial Atlantic and eastern Pacific, *Tellus, 29,*
523-529, 1977.

Hellerman, S. and M. Rosenstein, Normal monthly wind
stress ovet the world ocean with error estimates, *J. Phys.
Oceanogr., 13,* 1093-1104, 1983.

Hoffman, E. E., Plankton dynamics on the outer southeastern
U.S. continental shelf. Part III. A coupled physical-
biological model, *J. Mar. Res., 46,* 919-946, 1988.

Jenkins, W. J. and D. W. R. Wallace, Tracer based inferences
of new primary production in the sea, in *Primary
Productivity and Biogeochemical Cycles in the Sea,* edited
by P. G. Falkowski and A. D. Woodhead, Plenum, New
York, 1992.

Kawase, M. and J. L. Sarmiento, Nutrients in the Atlantic
thermocline, *J. Geophys. Res., 90,* 8961-8979, 1985.

Knox, F. and M. McElroy, Changes in atmospheric CO_2,
influence of marine biota at high latitudes, *J. Geophys.
Res., 89,* 4629-4637, 1984.

Levitus, S., Climatological atlas of the world ocean, *NOAA
Prof. Pap. 13,* Natl. Oceanic and Atmos. Admin., Boulder,
Colo., 1982.

Longhurst, A. R., Role of the marine biosphere in the global
carbon cycle, *Limnol. Oceanogr., 36,* 1507-1526, 1991.

Maier-Reimer, E. and K. Hasselmann, Transport and storage of
CO_2 in the ocean - an inorganic ocean circulation cycle
model, *Climate Dyn., 2,* 63-90, 1987.

Martin, J. H. and S. E. Fitzwater, Iron deficiency limits
phytoplankton growth in the north-east Pacific Subarctic,
Nature, 331, 341-343, 1988.

Martin, J. H., G. A. Knauer, D. M. Karl and W. W.
Broenkow, VERTEX: Carbon cycling in the northeast
Pacific, *Deep Sea Res., 34,* 267-285, 1987.

Martin, J. H., R. M. Gordon and S. E. Fitzwater, Iron in
Antarctic waters, *Nature, 345,* 156-158, 1990.

Miller, C. B., B. W. Frost, P. A. Wheeler, M. R. Landry, N.
Welschmeyer and T. M. Powell, Ecological dynamics in
the subarctic Pacific, a possibly iron-limited system,
Limnol. Oceanogr., 36, 1600-1615, 1991.

Najjar, R. G., J. L. Sarmiento and J. R. Toggweiler,
Downward transport and fate of organic matter in the
Oceans: Simulations with a general circulation model,
Global Biogeochem. Cycles, 6, 45-76, 1992.

Ogawa, H. and N. Ogura, Comparison of two methods for
measuring dissolved organic carbon in sea water, *Nature,
356,* 696-699, 1992.

Pacanowski, R. C. and S. G. H. Philander, Parameterization
of vertical mixing in numerical models of tropical oceans,
J. Phys. Oceanogr., 11, 1443-1451, 1981.

Packard, T. T., M. Denis and P. Garfield, Deep-Ocean metabolic CO_2 production: calculations from ETS activity, *Deep Sea Res.*, *35*, 371-382, 1988.

Platt, T. and C. L. Gallegos, Modelling primary production, in *Primary Productivity in the Sea*, edited by P. Falkowski, 339-361, Plenum, New York, 1980.

Platt, T., S. Sathyendranath, O. Ulloa, W. G. Harrison, N. Hoepffner and J. Goes, Nutrient control of phytoplankton photosynthesis in the Western North Atlantic, *Nature*, *356*, 229-231, 1992.

Riley, G. A., A theoretical analysis of the zooplankton population of Georges Bank, *J. Mar. Res*, *6*, 104-113, 1947.

Sarmiento, J. L., On the North and Tropical Atlantic heat balance, *J. Geophys. Res.*, *91*, 11,677-11,689, 1986.

Sarmiento, J. L. and J. R. Toggweiler, A new model for the role of the oceans in determining atmospheric pCO_2, *Nature*, *308*, 621-624, 1984.

Siegenthaler, U. and T. Wenk, Rapid atmospheric CO_2 variations and ocean circulation, *Nature*, *308*, 624-625, 1984.

Smith, S. D. and F. W. Dobson, The heat budget at Ocean Weather Ship Bravo, *Atmos. Ocean.*, *22*, 1-22, 1984.

Steele, J. H., Plant production in the northern North Sea, *Rep. 7*, Scot. Home Dep. Mar. Res. HMSO, Edinburgh, 1958.

Steele, J. H. and E. W. Henderson, The role of predation in plankton models, *J. Plankton Res.* *14*, 157-172, 1992.

Sugimura, Y. and Y. Suzuki, A high-temperature catalytic oxidation method for the determination of non-volatile dissolved organic carbon in seawater by direct injection of a liquid sample, *Mar. Chem.*, *24*, 105-131, 1988.

Suzuki, Y., Y. Sugiumura and T. Itoh, A catalytic oxidation method for the determination of total nitrogen dissolved in seawater, *Mar. Chem.*, *16*, 83-97, 1985.

Toggweiler, J. R., Is the downward dissolved organic matter (DOM) flux important in carbon transport?, in *Productivity of the Ocean: Present and Past*, edited by V. S. Smetacek, W.H. Berger and G. Wefer, 65-83, John Wiley, New York, 1989.

Toggweiler, J. R., J. L. Sarmiento, R. Najjar and D. Papadenetriou, Models of chemical cycling in the oceans: A progress report, *Tech. Rep. #4*, Ocean Tracers Lab., Princeton Univ., Princeton, N.J., 1987.

Walsh, J., Herbivory as a factor in patterns of nutrient limitaion in the sea, *Limnol. Oceanogr.*, *21*, 1-13, 1976.

Walsh, J. J. and C. P. McRoy, Ecosystem analysis in the southeastern Bering Sea, *Cont. Shelf Res.*, *5*, 259-288, 1986.

Walsh, J. J., D. A. Dieterle and M. B. Meyers, A simulation analysis of the fate of phytoplankton within the Mid-Atlantic Bight, *Cont. Shelf Res.*, *8*, 757-787, 1988.

Wroblewski, J. S., A model of phytoplakton plume formation during variable Oregon upwelling, *J. Mar. Res.*, *35*, 1977.

Yentsch, C. S., Estimates of new production in the mid-North Atlantic, *J. Plankton Res.*, *12*, 717-734, 1990.

Yoder, J. A., C. R. McClain, G. C. Feldman and W. E. Esaias, Annual cycles of phytoplankton chlorophyll concentration in the global ocean: a satellite view, *Global Biogeochem. Cycles*, *7*, 181-193, 1993.

H. W. Ducklow, Horn Point Environmental Laboratories University of Maryland Center for Environmental and Estuarine Sciences, Cambridge, MD 21613.

G. T. Evans, Department of Fisheries and Oceans, Science Branch St. John's, Newfoundland, Canada.

M. J. R. Fasham, Institute of Oceanographic Sciences Deacon Laboratory, Natural Environmental Research Council, Southampton SO1 7NS, United Kingdom.

J. L. Sarmiento and R. D. Slater, Program in Atmospheric and Oceanic Sciences, Princeton University, Princeton, NJ 08544

J. R. Toggweiler, Geophysical Fluid Dynamics Laboratory, NOAA, Princeton University, Princeton, NJ 08544